DOE/JPL-956999-85/1
[redacted]

IN-
CAT 44

DOE/JPL 956999-84/5
Distribution Category UC-63

DRL No. 220
DRD No. SE
Item No. 6

ADVANCED DENDRITIC WEB GROWTH DEVELOPMENT AND DEVELOPMENT OF SINGLE-CRYSTAL SILICON DENDRITIC RIBBON AND HIGH-EFFICIENCY SOLAR CELL PROGRAM

C. S. Duncan, R. G. Seidensticker,
J. P. McHugh, and R. H. Hopkins

FINAL REPORT

WORK PERFORMED FOR:

Jet Propulsion Laboratory
Contract No. 956999

August 29, 1986

Westinghouse R&D Center
1310 Beulah Road
Pittsburgh, Pennsylvania 15235

DOE/JPL-956999-85/1
9950-1196

DOE/JPL 956999-84/5
Distribution Category UC-63

DRL No. 220
DRD No. SE
Item No. 6

9950-1255-86/2

ADVANCED DENDRITIC WEB GROWTH DEVELOPMENT AND DEVELOPMENT OF SINGLE-CRYSTAL SILICON DENDRITIC RIBBON AND HIGH-EFFICIENCY SOLAR CELL PROGRAM

C. S. Duncan, R. G. Seidensticker,
J. P. McHugh, and R. H. Hopkins

FINAL REPORT

WORK PERFORMED FOR:

Jet Propulsion Laboratory
Contract No. 956999

August 29, 1986

Westinghouse R&D Center
1310 Beulah Road
Pittsburgh. Pennsylvania 15235

TECHNICAL CONTENT STATEMENT

Portions of this report were prepared as an account of work sponsored by the United States Government. Neither the United States nor the United States Department of Energy, nor any of their employees, nor any of their contractors, subcontractors, or their employees makes any warranty, expressed or implied, or assumes any legal liability or responsibility for the accuracy, completeness, or usefulness of any information, apparatus, product, or process disclosed, or represents that its use would not infringe privately owned rights.

This report was prepared for the Jet Propulsion Laboratory, California Institute of Technology, sponsored by the National Aeronautics and Space Administration.

CONTENTS

LIST OF FIGURES

LIST OF TABLES

1. INTRODUCTION AND SUMMARY

This report summarizes work performed on JPL Contract 956999, "Development of Single-Crystal Silicon Dendritic Ribbon and High-Efficiency Solar Cells." The contract was initiated September 12, 1984 and was completed on December 31, 1984. Work reported herein was completed under a "Partial Order Transfer" from the Westinghouse Advanced Energy Systems Division to the Westinghouse Research and Development Center. The bulk of this work was performed at the R&D Center, and this report represents work performed both at the R&D Center and at AESD.

Work performed under this contract was, in fact, a direct extension of work performed under JPL Contract 955843. This effort has continued into 1985 under yet another contract (957207). The long-range objectives of all these contracts are the same: to conduct development efforts to achieve initial deliverables of a JPL program aimed at demonstrating that the silicon dendritic web technology is ready for commercial use by the end of 1986. A commercial readiness goal involves improvements to crystal growth furnace throughput to demonstrate an area growth rate of greater than 15 cm^2/min while simultaneously growing 10 meters or more of ribbon under conditions of continuous melt replenishment. "Continuous" means that the silicon melt is being replenished at the same rate that it is being consumed by ribbon growth so that the melt level remains constant.

Specific tasks of this contract No. 956999 included computer thermal modeling required to define high-speed, low-stress, continuous growth configurations; a study of convective effects in the molten silicon and growth furnace cover gas; furnace component modifications; web quality assessments; and experimental growth activities to

demonstrate progress. A specific milestone identified in this contract involved demonstration of an area growth rate greater than 10 cm^2/min while simultaneously growing 10 meters or more of ribbon under conditions of continuous melt replenishment by the end of 1984.

Overall progress toward achieving increased crystal lengths in this as well as previous related contracts dating from 1980 is presented in Figure 1. Crystal lengths of up to 10.9 meters were achieved prior to the end of 1984 during growth with no replenishment. Replenished growth configurations have produced crystals up to 7 meters -- the 1984 goal being 10 meters.

Figure 2 further elaborates on progress made in the web growth program in 1984 (this contract covering the last three-month portion of the year) toward goals in continuously replenished crystal growth. The maximum crystal length grown in a melt replenishment mode prior to March 1984 was 2 meters; the crystal required three hours of growth time. Through the course of this program, crystal lengths have more than tripled; growth times, before interruption of growth due to the onset of thermal instability, have increased by almost a factor of four.

The 1984 web growth goals of crystal length and time are also presented in Figure 2. A comparison will show that stability improvements to increased uninterrupted growth times have exceeded the goals. However, crystal pull speeds have not increased as was hoped, resulting in shorter crystals than projected. The pull speed is limited by stresses in the growing crystal that can themselves interrupt growth. As a result of work completed on this contract, the primary focus of the 1985 Web Growth Development Program is being directed toward the solution of the stress problem.

The overall status of the Web Growth Development Program at the end of 1984 is presented in Table 1.

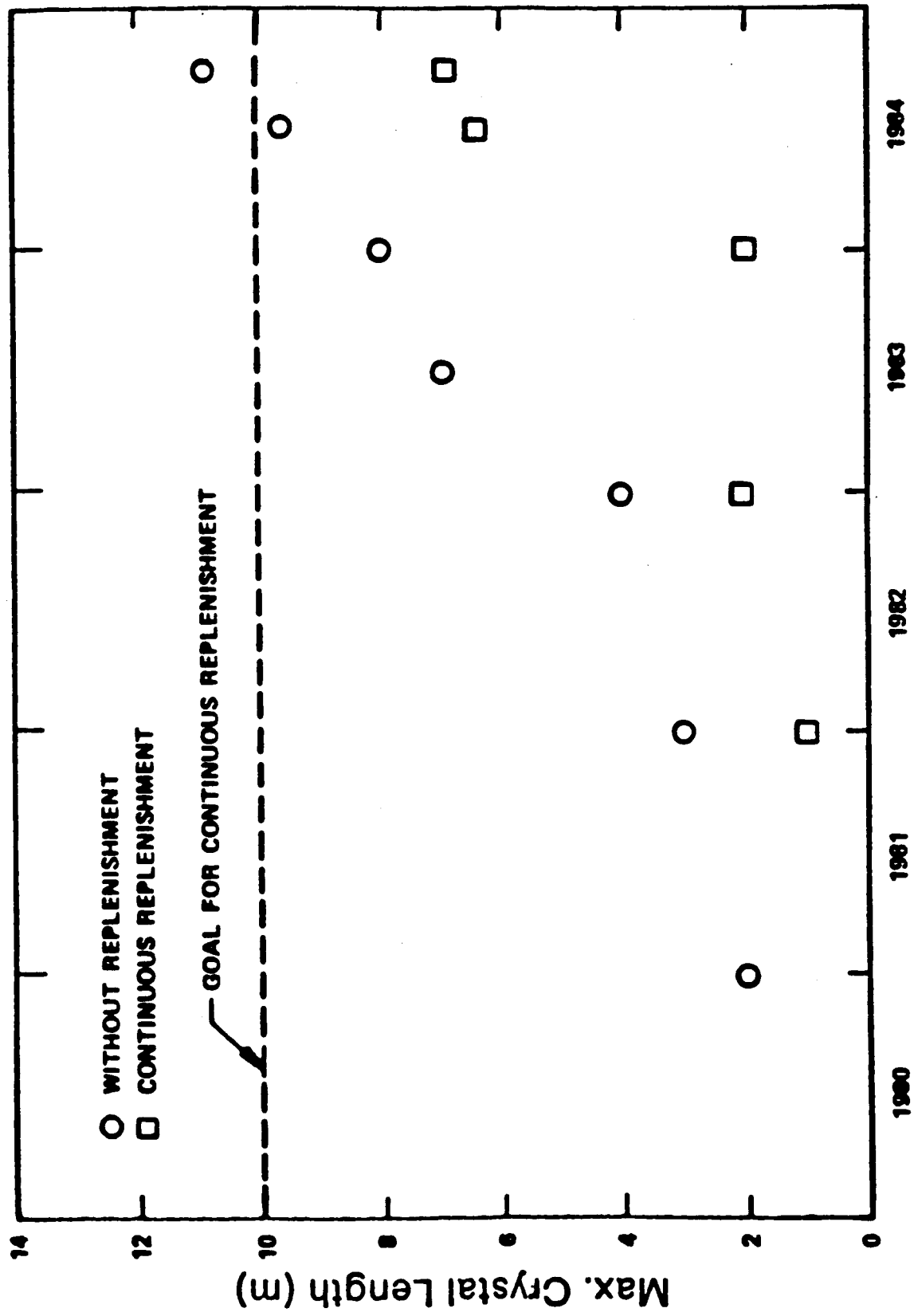

Figure 1. Progress made toward growth of long crystals.

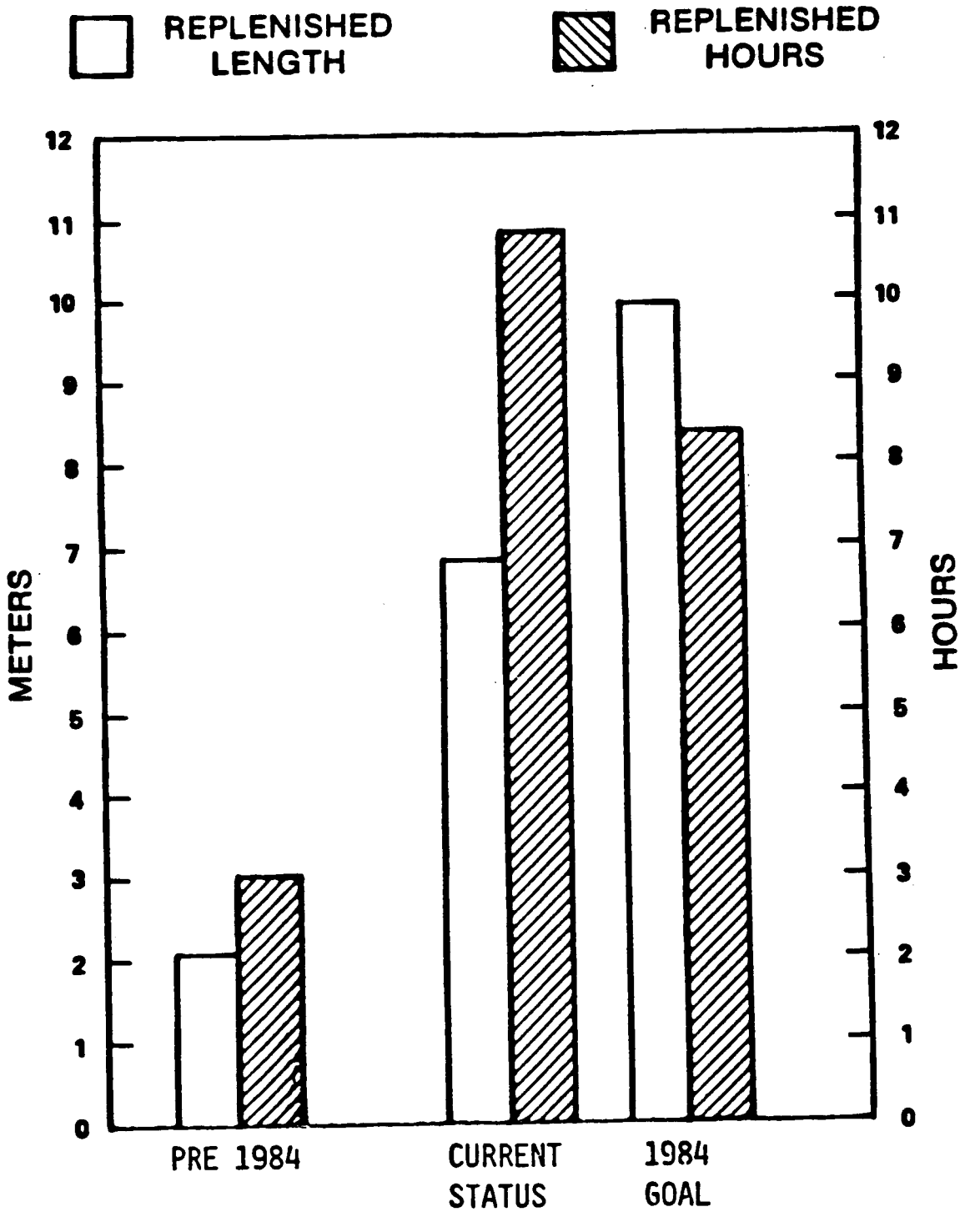

Figure 2. Continuously replenished web growth.

Table 1. Web Growth Development Status -- December 1984

- Primary Thermal Variable Identified and Fix Verified
- Significantly Improved Thermal Isolation of Growth and Melt Regions Achieved
- 6.8 m Long Ribbon Grown at 7 cm^2/min Rate with Replenishment
- Replenished Web Production Equivalent to Pre-Pilot Line Furnaces
- Computer Based Data System Being Used to Assist in Parameter Correlations
- 10 m Long Crystal Grown
- Additional Stress Reduction Work Required to Achieve 10 cm^2/min Rate

2. TECHNICAL PROGRESS

2.1 Thermal Stress and Buckling Modeling

Modeling of thermal stresses and buckling of dendritic web crystals during growth operations is required to define growth configurations capable of continuous production of high-quality ribbon (having suitable thickness and low stress) at increased area growth rates. In particular, the ultimate goal of this contract was to demonstrate an area growth rate of greater than 10 cm^2/min while simultaneously growing 10 meters or more of ribbon under conditions of continuous melt replenishment.

Experimental temperature data from elements of a state-of-the-art growth configuration (labeled J460) were used as input for initial modeling work. The experiments were performed prior to initiation of this contract. Previous modeling of the J460 growth configuration has been performed using calculated element temperatures. The principal differences were that the newer cases had a much colder second lid (L2) and a somewhat hotter shield stack than in previous models. Results of the initial calculations performed using experimental temperature data indicated that the growth velocity increased by about 16% (compared to previous calculations) but that interface stress had concurrently increased about 40%. The far stress peak, a principal source of buckling, decreased by about 40%. While these results indicated the sensitivity of growth parameters to lid temperature changes, it was felt to be too drastic a change in L2 temperature. Accordingly, plans were made to check the temperature data for the second lid using optical pyrometry.

Based on the effect of the hotter stack temperature, a modification of the J460 configuration was modeled to include a vertical thermal

element on the top of the normal shield stack. The calculated temperature profile for the modified configuration indicated that the far stress peak should be almost eliminated. Stress calculations were initiated; set-up of an experimental furnace to check the results was also initiated.

Difficulties were encountered in performing a stress or buckling configuration for the modified configuration as a result of operating system changes in the computers at the Westinghouse Nuclear Center where the WECAN code is run. To allay this problem, the temperature calculation code was transferred from the Univac 1180 (at the Westinghouse R&D Center) to the Cray-1 (at the Westinghouse Nuclear Center), allowing direct interface with the CDC7600 that runs the WECAN stress and buckling programs.

In addition, stress modeling calculations were made to investigate the effect of an asymmetric variation of temperature across the width of the ribbon and thus complete the investigation of lateral temperature variations in web crystal growth. Two cases were considered.

In the first case, a linear variation in temperature was imposed across the width of the crystal. In the second case, a cubic variation in temperature was imposed across the width. In both cases, the absolute temperature difference between the centerline and the dendrites was ten degrees as in the previous cases. The temperature profile was assumed to be:

$$T(x,y) = T(x)g(y) \tag{1}$$

where T(x) is expressed mathematically by:

$$T(x) = (A/B^2)\exp(-Bx) + Cx + D. \tag{2}$$

In these expressions, A, B, C, and D are constants, x is the position along the length of the crystal measured from the solid-liquid interface, and y is measured across the ribbon width from the centerline.

The y-variation of temperature functions used were:

$$g(y) = 1 + .00593\ (y/w) \tag{3}$$

and

$$g(y) = [1 + .00593(y/2)^3]/(1.0015). \tag{4}$$

In these expressions, w is the ribbon half-width.

A significant difference between the calculations performed here and any previous ones, at least from the point of computation time, was the necessity of using a full-width mesh as shown in Figure 3. The extraction of the first and second eigenvalues (buckling modes) increased the computer time approximately four-fold over the earlier cases. The stresses in the case of the isotherms with a linear y-variation were very similar to those calculated previously in models in which no y-variations in temperature were considered. This should not be surprising since the linear y-variation in temperature would not change the Laplacian of the temperature. There was some change in the stress pattern for the cubic case with the stress increasing on one side and decreasing on the other. Again, this effect can be understood in terms of the effect of the y-variation of the temperature.

The buckling results are somewhat more surprising. The eigenvalues for both symmetric and antisymmetric buckling (bending and twisting) are given in Table 2.

Considering that the numerical algorithm currently used for extracting the eigenvalues is different from that used when the flat isotherm case was analyzed, the small variations in the numerical values are insignificant. The lack of any effect from the linear y-variation is reasonable since the stress profiles are not affected as noted. The insensitivity of buckling to the cubic y-variation is more surprising and might be attributed to the lack of any significant net change in the stress across the width of the ribbon.

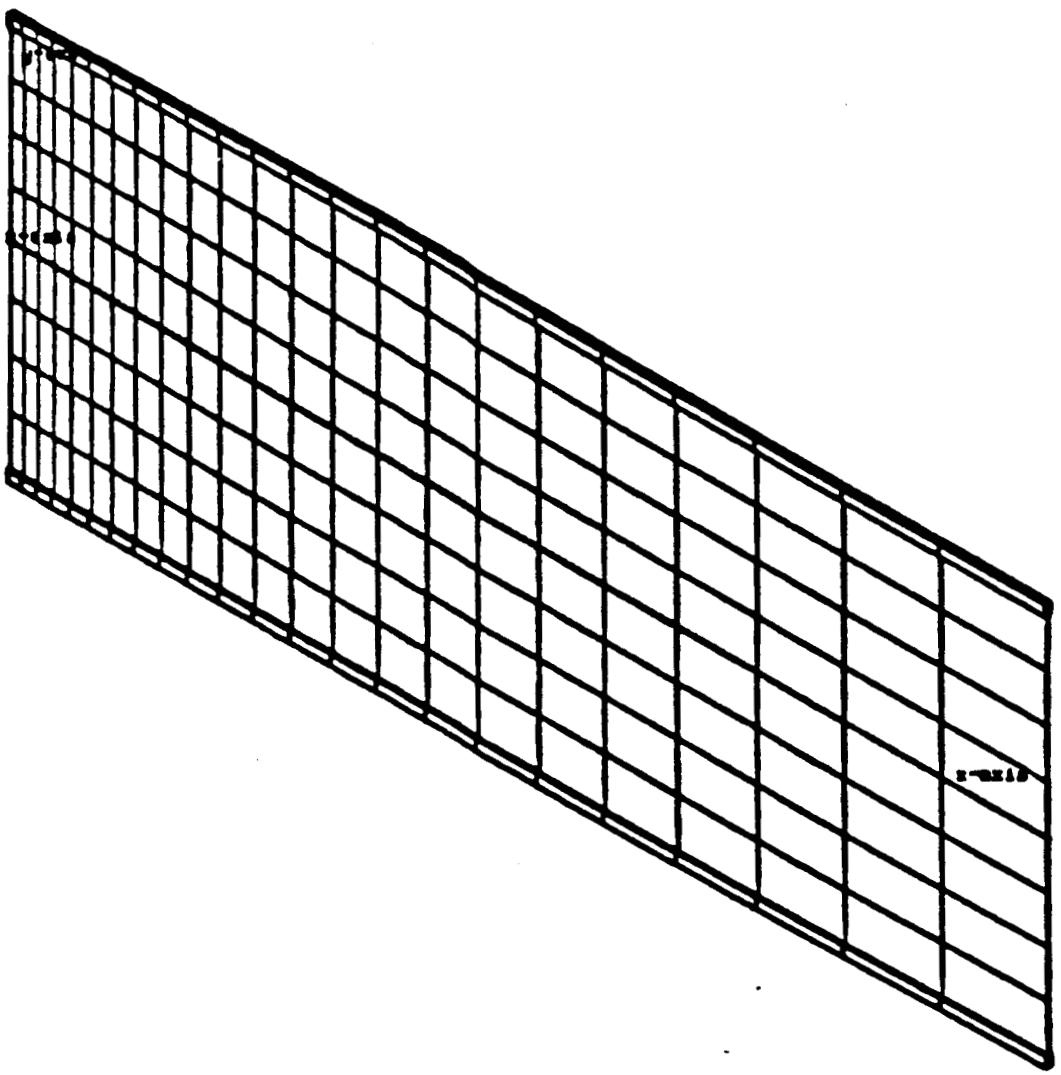

Figure 3. Full width WECAN mesh for buckling analysis.

Table 2. Buckling Eigenvalues

Case	Eigenvalue	
	Symmetric	Antisymmetric
Flat Isotherms	1.467	1.597
Linear slope in y	1.448	1.568
Cubic in y	1.445	1.565

These results have an important implication for the actual growth of the web ribbons in that the asymmetry of the temperature profile across the width of the ribbon has negligible effect compared to the temperature profile along the length of the ribbon, and for any positive or negative net curvature of the isotherms that may exist.

Analytical work was completed on this contract using a "first-order" approach which involved use of separate models to describe various aspects of the dendritic web growth system. Aspects considered involve temperature distribution in the web crystal during growth, stress in the web crystal resulting from these temperature distributions, fluid flow in the crucible containing the molten silicon, and the temperature distribution in the molybdenum susceptor that heats the silicon.

Figure 4 is a logic diagram that shows how the web temperature and stress analysis are coupled in the "first-order modeling" technique.

Table 3 summarizes the most significant results achieved in 1984 through the use of the first-order modeling. Conclusions concerning the continued use of the first-order approach are summarized in Table 4.

Based on these results and conclusions, a more comprehensive approach has been identified for use in future programs. This approach would integrate existing models so that a single model could be used for analyzing the web growth system (with the exception of the stress/buckling calculations). The advantage would be that the system

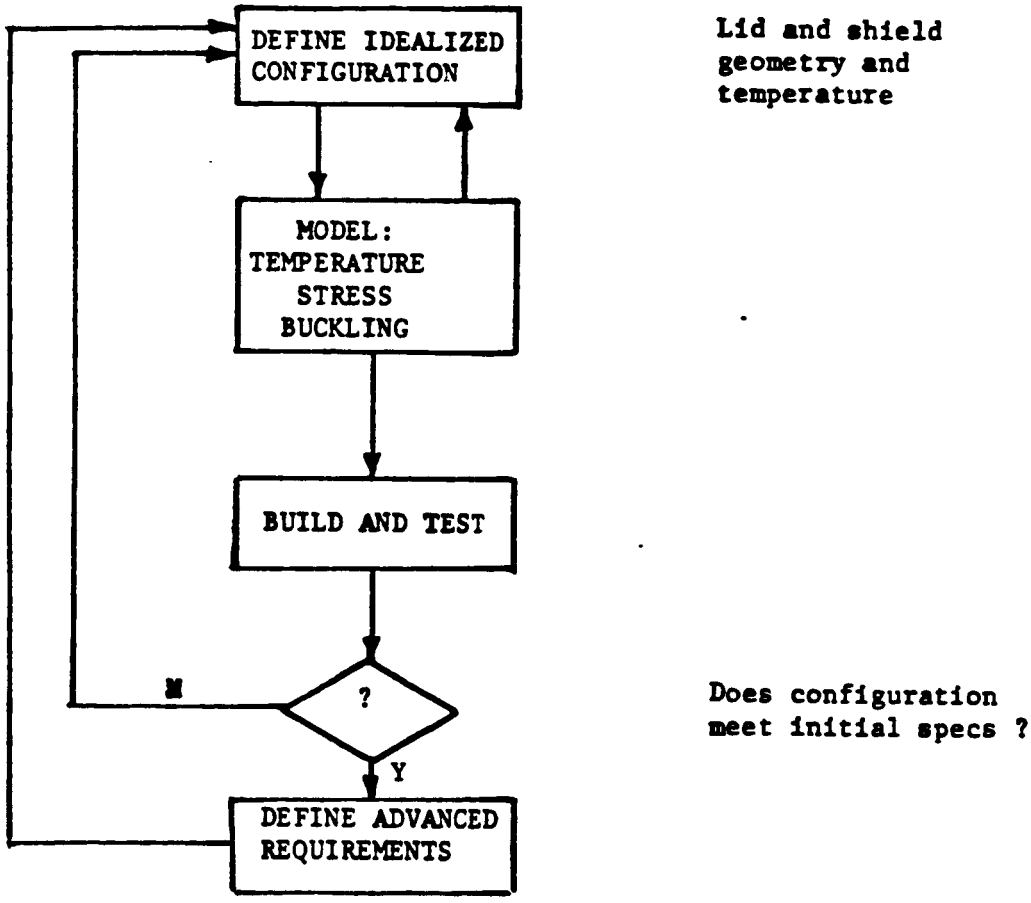

Figure 4. Logic Diagram of First Order Modeling Approach.

Table 3. Results of First Order Modeling

1. Hardware developed on basis of modeling:
   a. Grows web crystals 5 to 6 cm wide
   b. Grows web crystals at 2 to 3 cm/min
   [But not simultaneously on a long-term basis.]
2. Model predictions validated when real system temperatures are used for boundary conditions.
3. Model has predicted a design for simultaneous growth at $W > 5$ cm and $V > 2$ cm/min.
4. Highest speed growth configurations can produce crystals with large residual stress.
   [Residual stress generation is not included in model, but has not been a problem to date.]
5. Simultaneous satisfaction of the required boundary conditions for web temperature and melt temperature can be complex.

Table 4. Calculations Based on First Order Modeling

1. Interactions of system elements is becoming more important with more advanced systems.
2. A more comprehensive analytical model is required for guidance in the integrated design of growth systems.
3. The significance of residual stress is not yet determined.

interactions could be readily evaluated and the design and evaluation process speeded up. Additionally, the more complete model would allow calculation of the effects of system changes that are presently accessible only by time-consuming experimental iterations. A logic diagram of the advanced modeling concept is shown in Figure 5.

The three-step procedure used in this program to analyze stress and buckling in growing dendritic web is outlined in Table 5. The

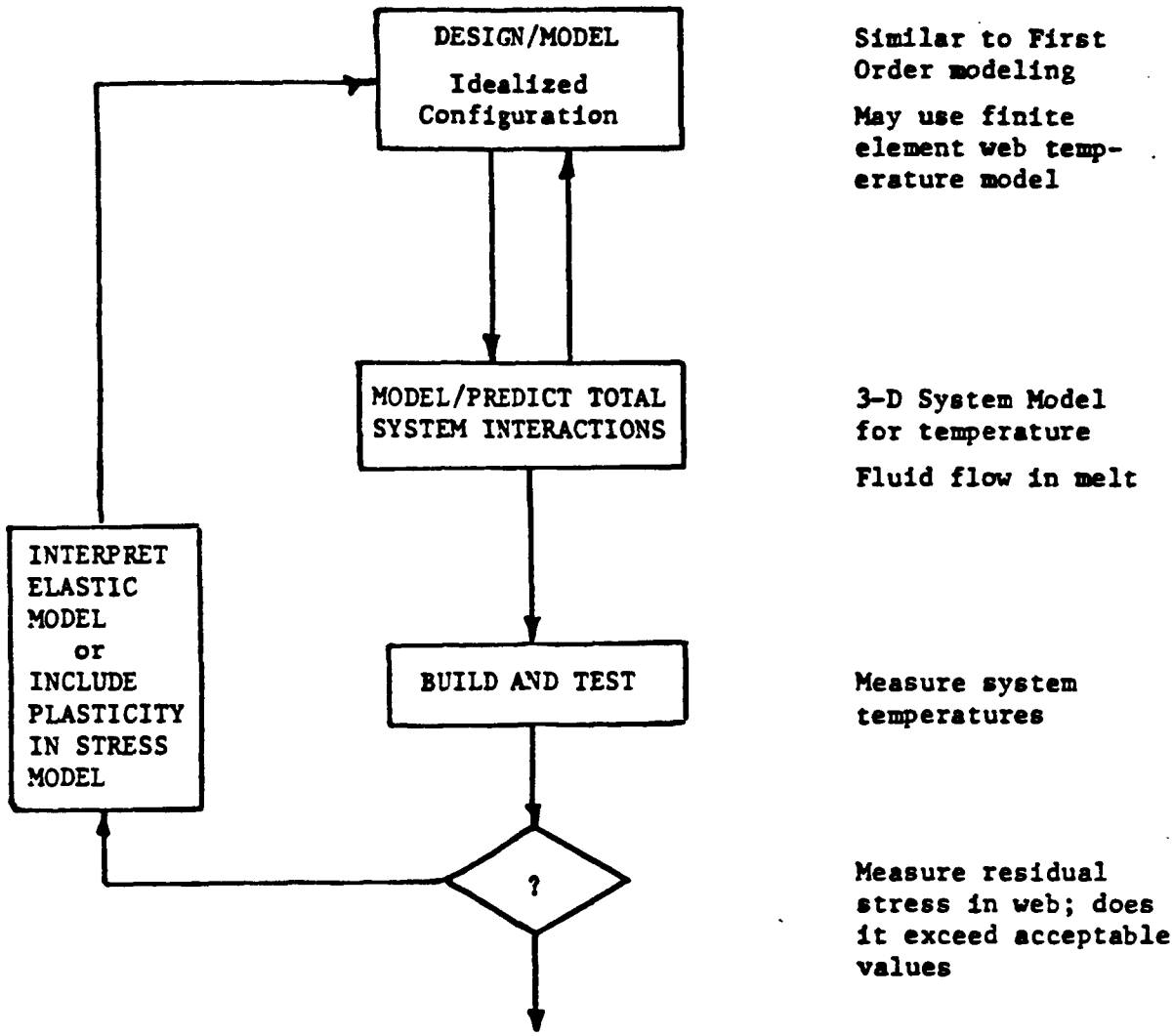

Figure 5. Logic diagram of advanced modeling approach.

Table 5. Three-Step Procedure for Analyzing Silicon Ribbon

- Step 1 -- Determining Temperature Profile
- Step 2 -- Performing Thermal Stress Analysis Using Temperature Profile Obtained From Step 1

  $[K]\{\Delta\} = \{F\}$

  $\{\sigma\} = [E][D]\{\Delta\}$
- Step 3 -- Performing Buckling Analysis

  $[K]\{\Delta\} = \lambda[K_s]\{\Delta\}$

  $\lambda < 1$ buckled

  $\lambda > 1$ not buckled

stress analysis is completed using the Westinghouse "WECAN" computer model. Basic capabilities of the model are summarized in Table 6. Figures 6 and 7 show the two- and three-dimensional element mesh capabilities, respectively, of the WECAN code.

Effects of asymmetric temperature variations in the y-direction (across the width) of the growing web were analyzed using the WECAN model. The two temperature variations imposed for this analysis are listed in Table 7. Computer-printed stress contours associated with the linear temperature variation are shown in Figure 8. These results are essentially identical to stress contours calculated in a previous program using flat isotherms.

Stress contours calculated using the asymmetric cubic temperature variation are shown in Figure 9. The asymmetry of the cubic contours is evident in the figure. Surprisingly, the critical buckling conditions were unaffected by the y-direction temperature profiles imposed across the width of the web.

The calculated ribbon shapes for the symmetric and asymmetric temperature variations are shown in Figures 10 and 11, respectively. Again, critical buckling shapes are essentially identical to those for the flat isotherm case.

Table 6. WECAN Analysis Capabilities

- Static Analysis
  - Elastic
  - Inelastic (Plasticity and Creep)
  - Large Deformation Prebuckling Analysis
- Thermal and Flow Analysis
  - Steady State and Transient Heat Conduction Analysis
  - Steady State Flow Analysis
  - Other Field Problems (Electromagnetic, etc.)
- Dynamic Analysis
- Harmonic Response Analysis
- Nonlinear Transient Dynamic Analysis
- Linear Buckling Analysis

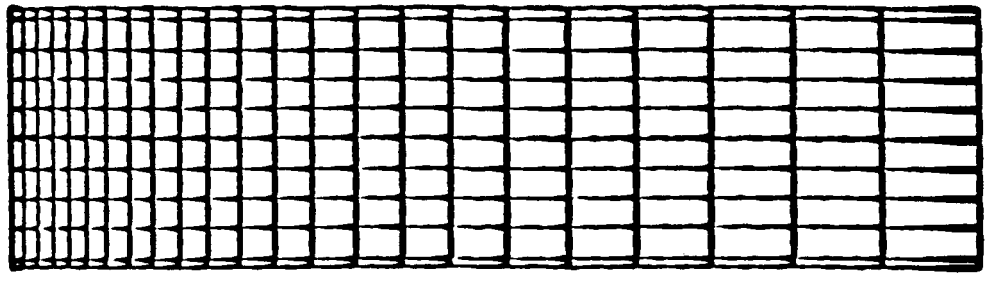

Figure 6. WECAN variable spacing finite element mesh.

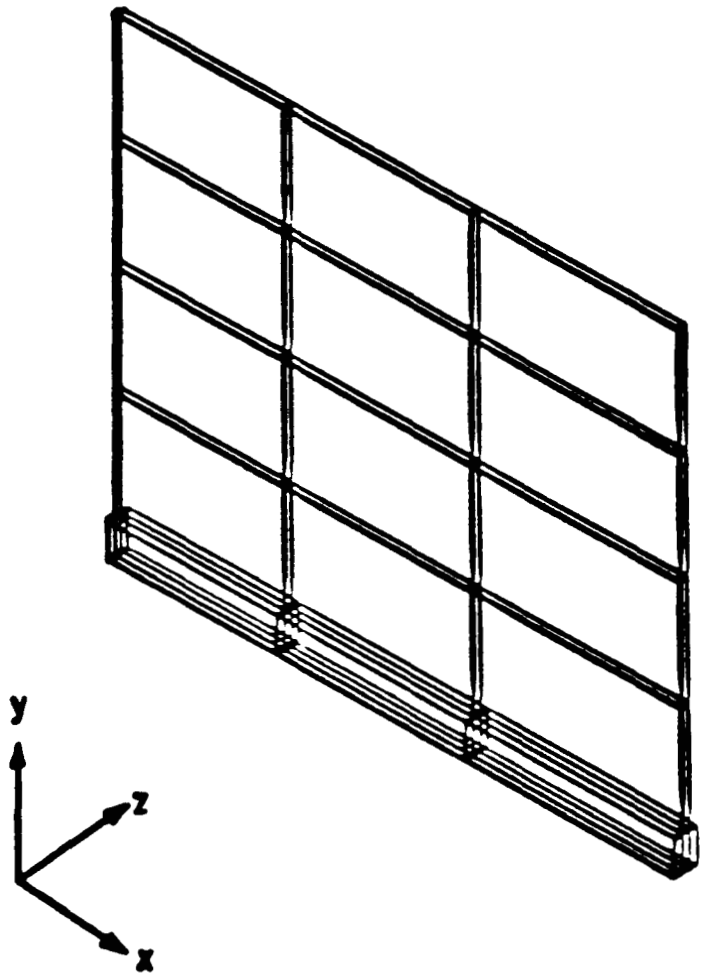

Figure 7. WECAN three-dimensional finite element mesh.

2.2 Liquid Convection and Heat-Transfer Modeling

The purpose of this task was to develop a quantitative understanding of convection and heat transfer in the liquid pool of silicon during dendritic web growth, with the ultimate objective of aiding both process optimization and the evolution of an optimal design. Work on this task was performed under subcontract to Cambridge Materials Modeling Group (CMMG) directed by Prof. Julian Szekely. Most of the work was performed by N. El-Kaddah of CMMG.

Table 7. Y-Direction Web Temperature Variation

$T(X,Y) = TM(X) \neq F(Y)$

WHERE

$TM(X) = (A/B\neq\neq 2) \neq EXP(-BX) + CX + D$

$F(Y) = 1 + C1 \neq (Y/W) + C3 \neq (Y/W) \neq\neq 3$

CASE 1 - LINEAR VARIATION (C3=0)

A = 3000, B = 5, C = -86.5 AND D = 1565

THIS IMPLIES THAT TM(0) = 1685 AND TM(10) = 700.

C1 = 0.00593 WHICH IMPLIES THAT T(0, 1.975) - T(0, 0) = 10

CASE 2 - CUBIC VARIATION (C1=0)

A, B, C AND D ARE SAME AS CASE 1.

C3 = 0.0593 WHICH IMPLIES THAT T(0, 1.975) - T(0, 0) = 10

The domain of interest of this work is sketched in Figure 12. The walls of the crucible are heated while a thin film of silicon monocrystal (dendritic web) is being withdrawn, as also illustrated in the sketch.

The objective of this analysis was to define convection within the liquid pool. This convection plays an important role in affecting the temperature field and its stability in the vicinity of the dendrites at the leading edge of the solid film, as the crystal is being withdrawn. This analysis was intended to lead to an understanding of techniques required to increase both the film withdrawal speed and the film width while minimizing convection in the molten silicon.

In the initial phase of the convection modeling work it was suggested that the most critical temperature distribution was probably in the cross section of the melt normal to the plane of the web crystal,

Figure 8. Stress contours for linear Y-temperature profile.

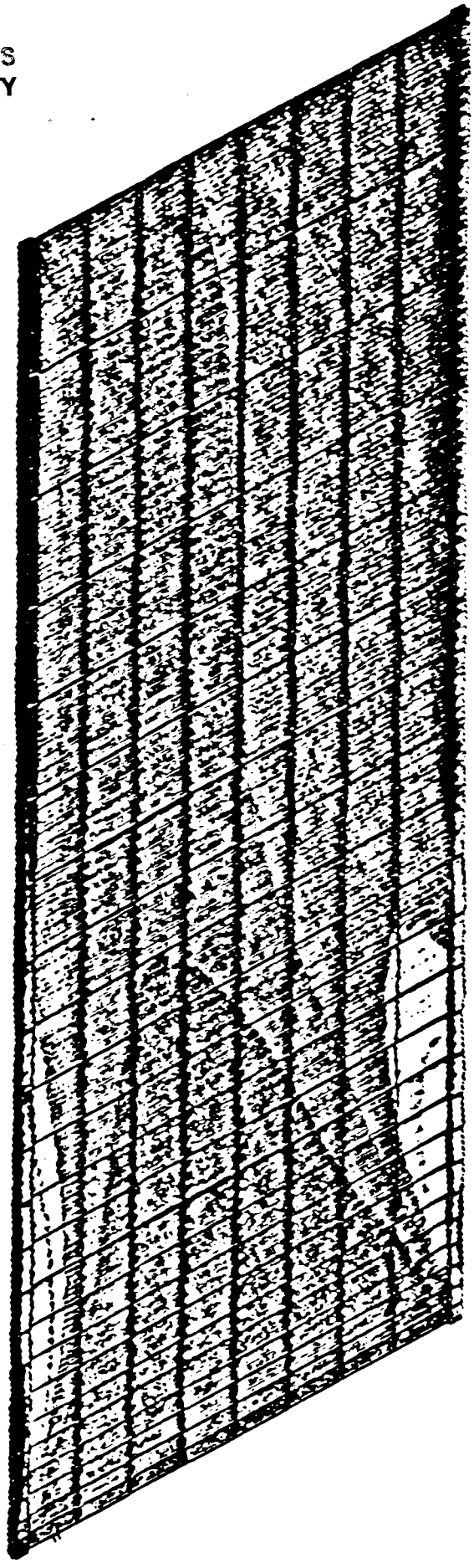

Figure 9. Stress contours for asymmetric cubic Y-temperature profile.

Figure 10. Calculated ribbon shape for symmetric temperature variation.

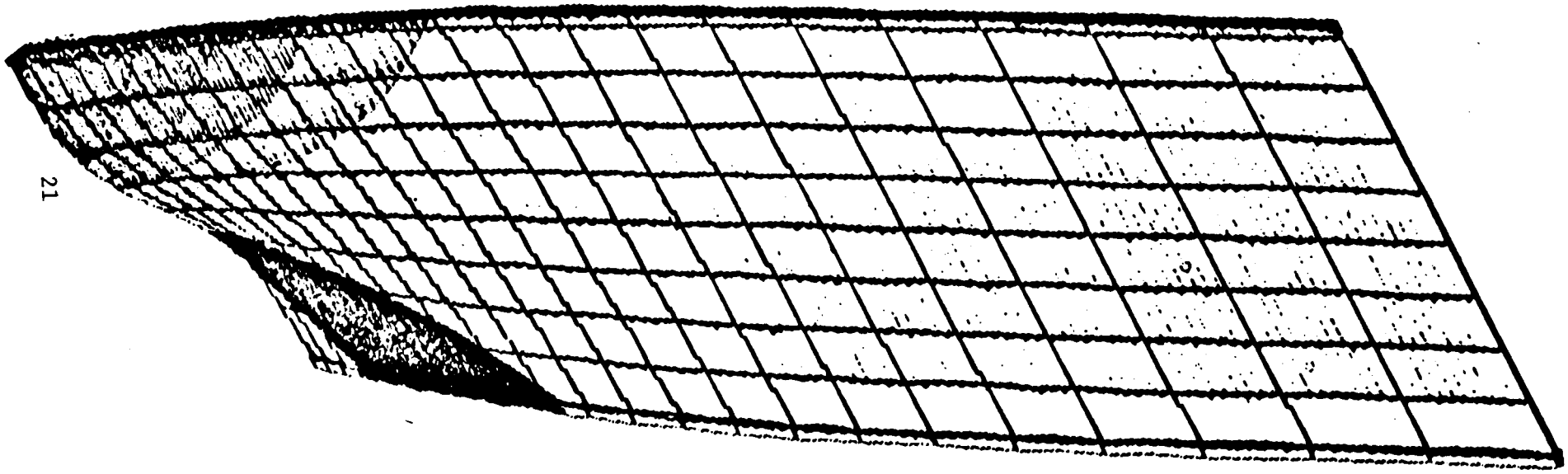

Figure 11. Calculated ribbon shape for asymmetric temperature variation

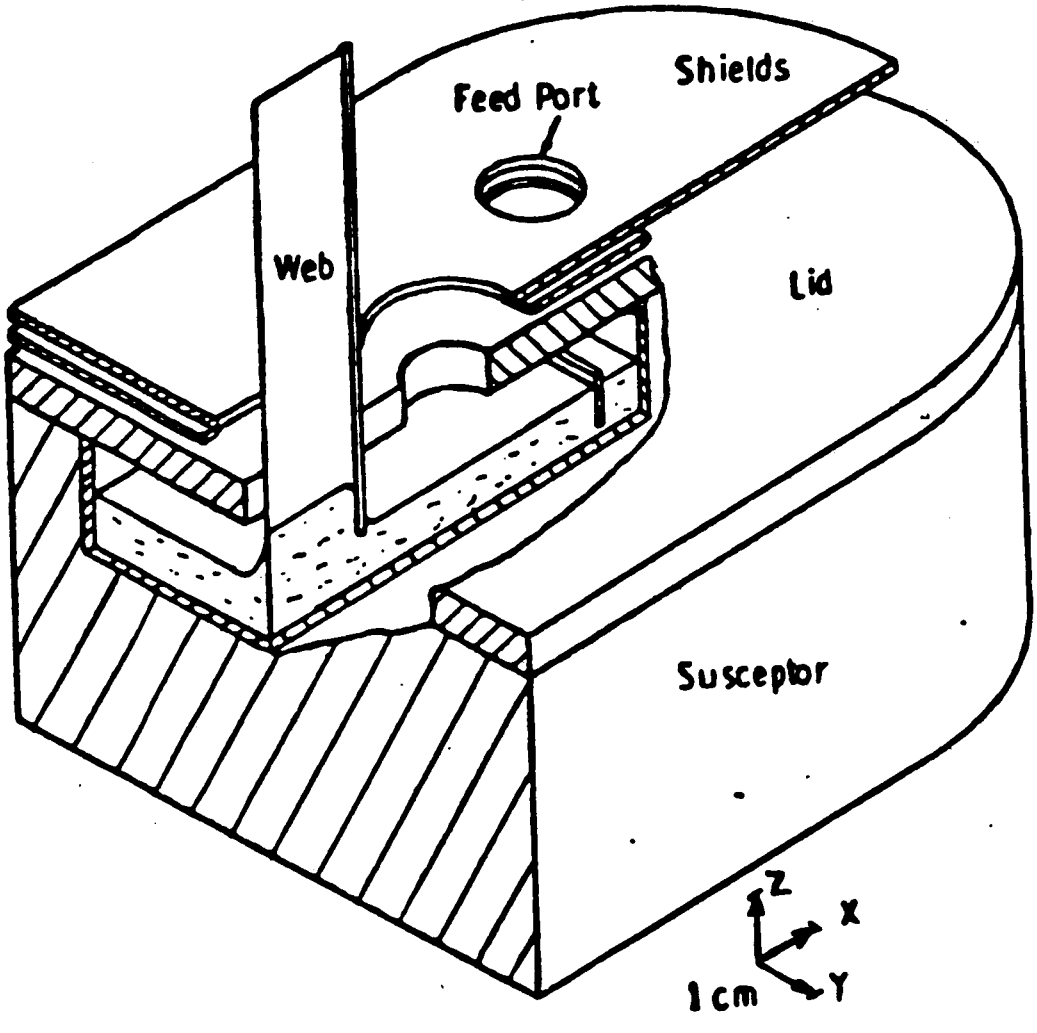

Note: Coordinate system is different than that used in stress analysis.

Figure 12. Sketch of the growth region in a dendritic web furnace.

and a hypothetical, but reasonable, temperature field was selected for this region. Using this field as the input data, Szekely and El-Kaddah calculated the fluid flow in the silicon melt. A typical example is shown in Figure 13, where the temperature field is shown at the top of the figure. In the particular case illustrated, a melt depth of 0.9 cm was assumed. A similar calculation was made for a melt depth of 0.7 cm. The contrast between the two cases was striking. The 0.2 cm reduction in melt depth resulted in a decrease in the maximum flow velocity by a factor of two. This change is in qualitative agreement with the experimental observation that reducing the melt height by a millimeter or so greatly improves the stability of web growth.

Parametric variations were then studied to provide a basis for possible future crucible designs. Parameters selected for evaluation were crucible width, length, and temperature asymmetry. In addition, a different temperature profile, calculated from a two-dimensional WECAN model of the growth system, was provided as input for evaluation. Although this temperature field was qualitatively similar to the one used for the initial flow calculations, it was quantitatively different such that resulting flow patterns would give some indication of the sensitivity of the system to the details of the temperature field.

The two-dimensional mesh shown in Figure 14 was used to calculate the temperature field in the whole furnace system (although the melt was, of course, the region of particular interest in this analysis). For simplicity, radiation connections between elements are not shown in the figure. Input data for the initial exercise of the model was the measured temperature profile shown in Figure 15. The resulting melt temperature distribution is shown in Figure 16.

The second case run with the model was a parametric variation in which the emissivity of the silicon melt and the molybdenum surface elements were increased by 50%, i.e., from 0.2 to 0.3. The same temperature profile (Figure 15) was used as the input data for the second run. The resulting melt temperature distribution is shown in

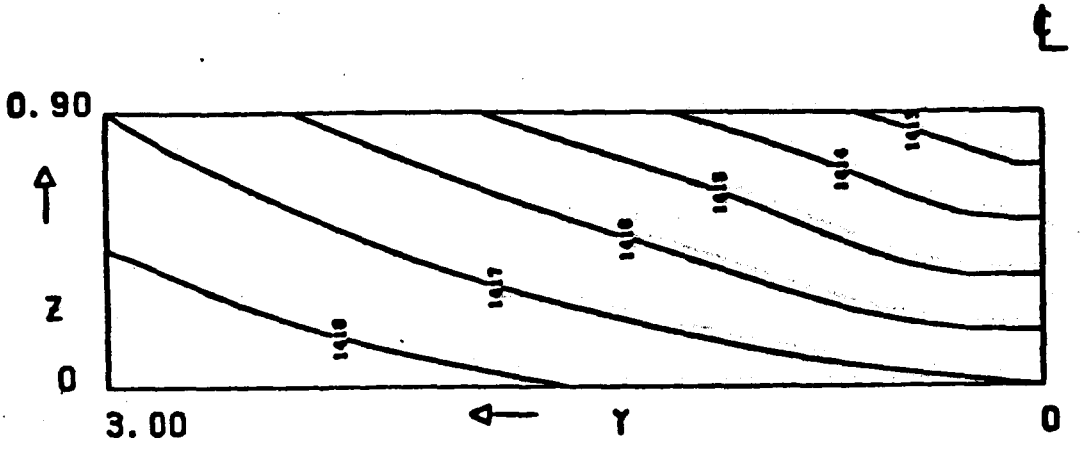

A. Calculated Temperature Field for a 9 mm Melt Deep Silicon Melt

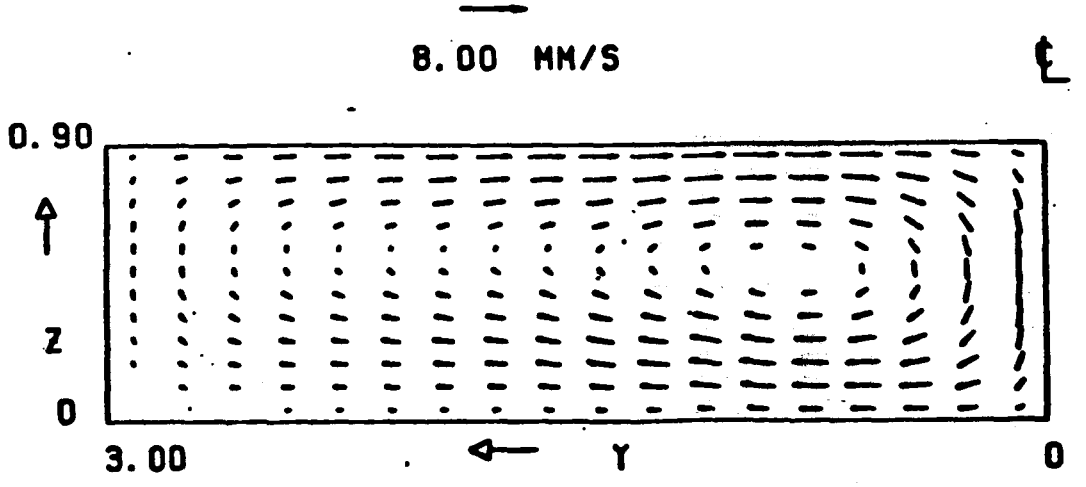

B. Calculated Velocity Field for a 9 mm Melt Deep Silicon Melt

Figure 13. Calculated temperature and velocity fields in a silicon melt (from Szekely and El-Kaddah).

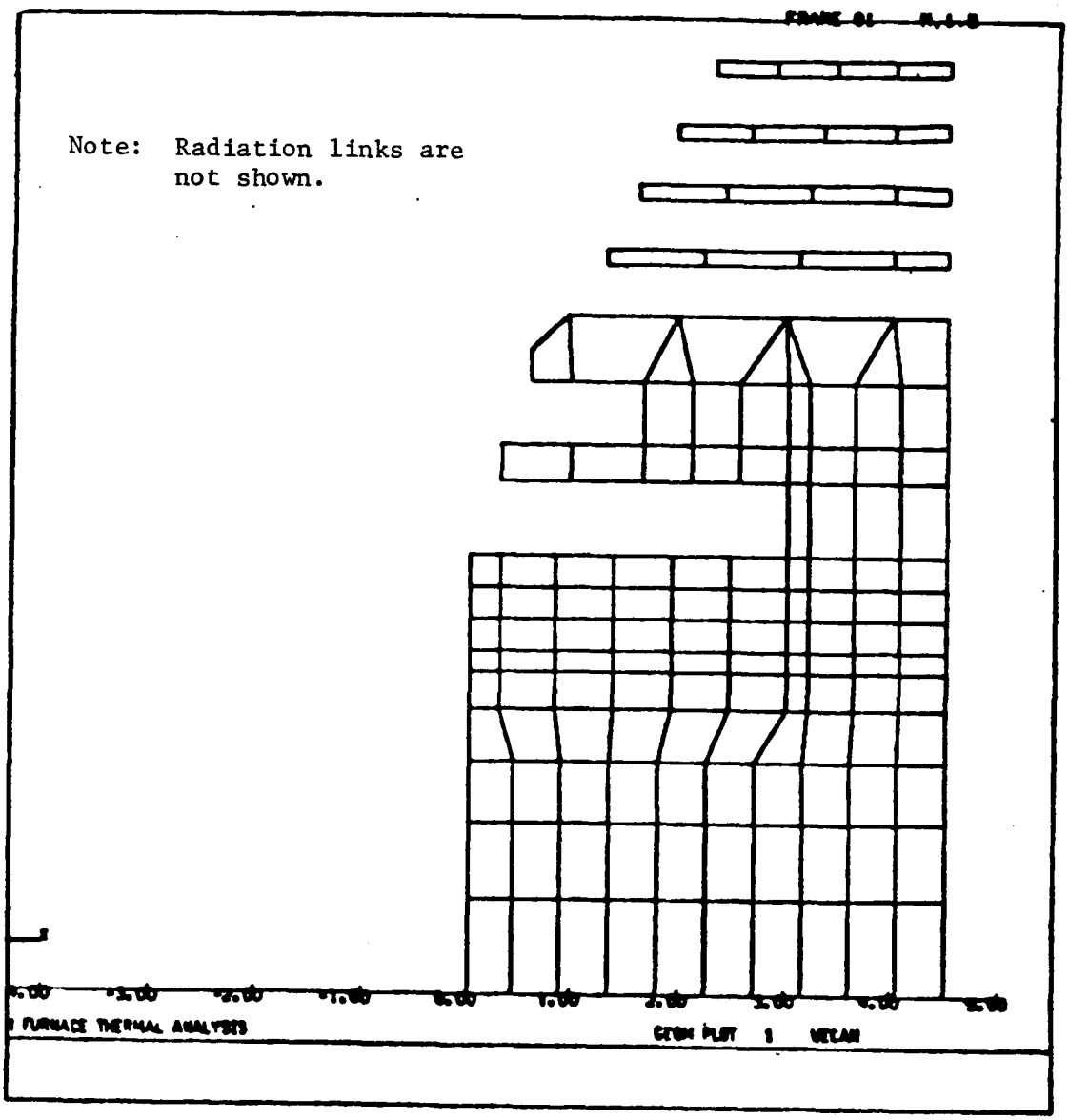

Figure 14. Finite element mesh for analysis of web growth system.

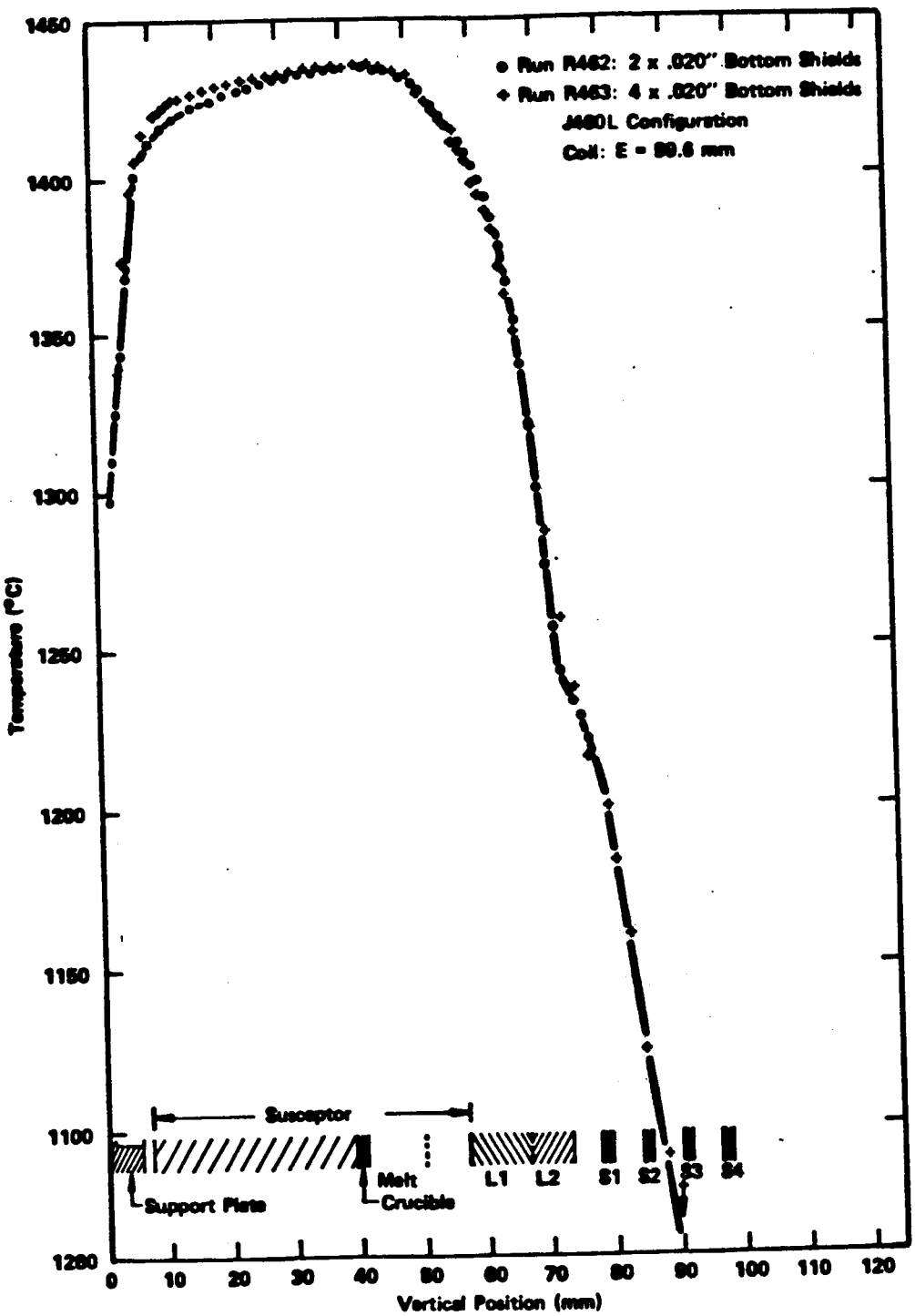

Figure 15. Temperature profile used as input data for finite element analysis.

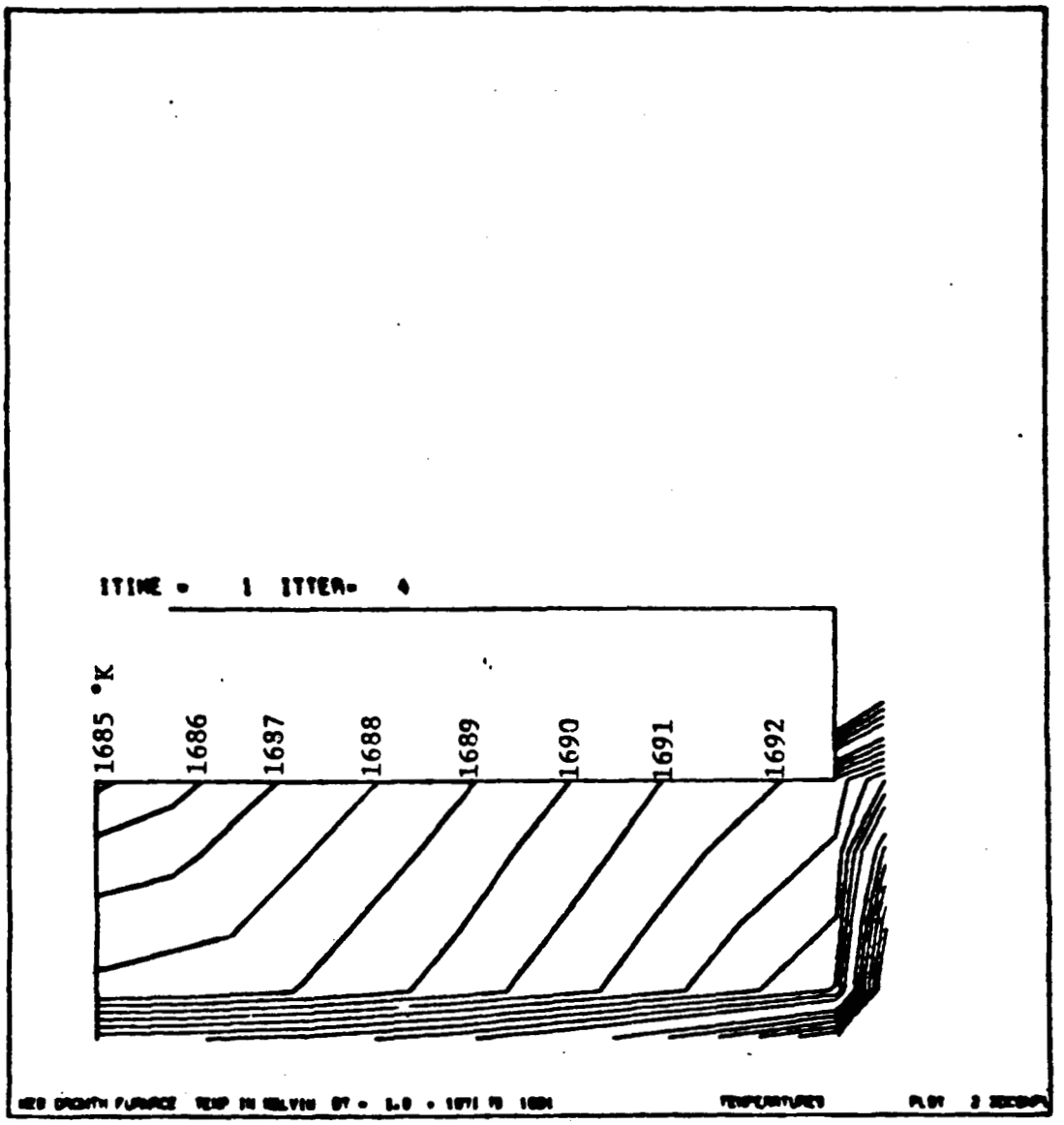

Figure 16. Isotherms in silicon melt resulting from temperature input of Figure 15 when $\varepsilon = 0.2$.

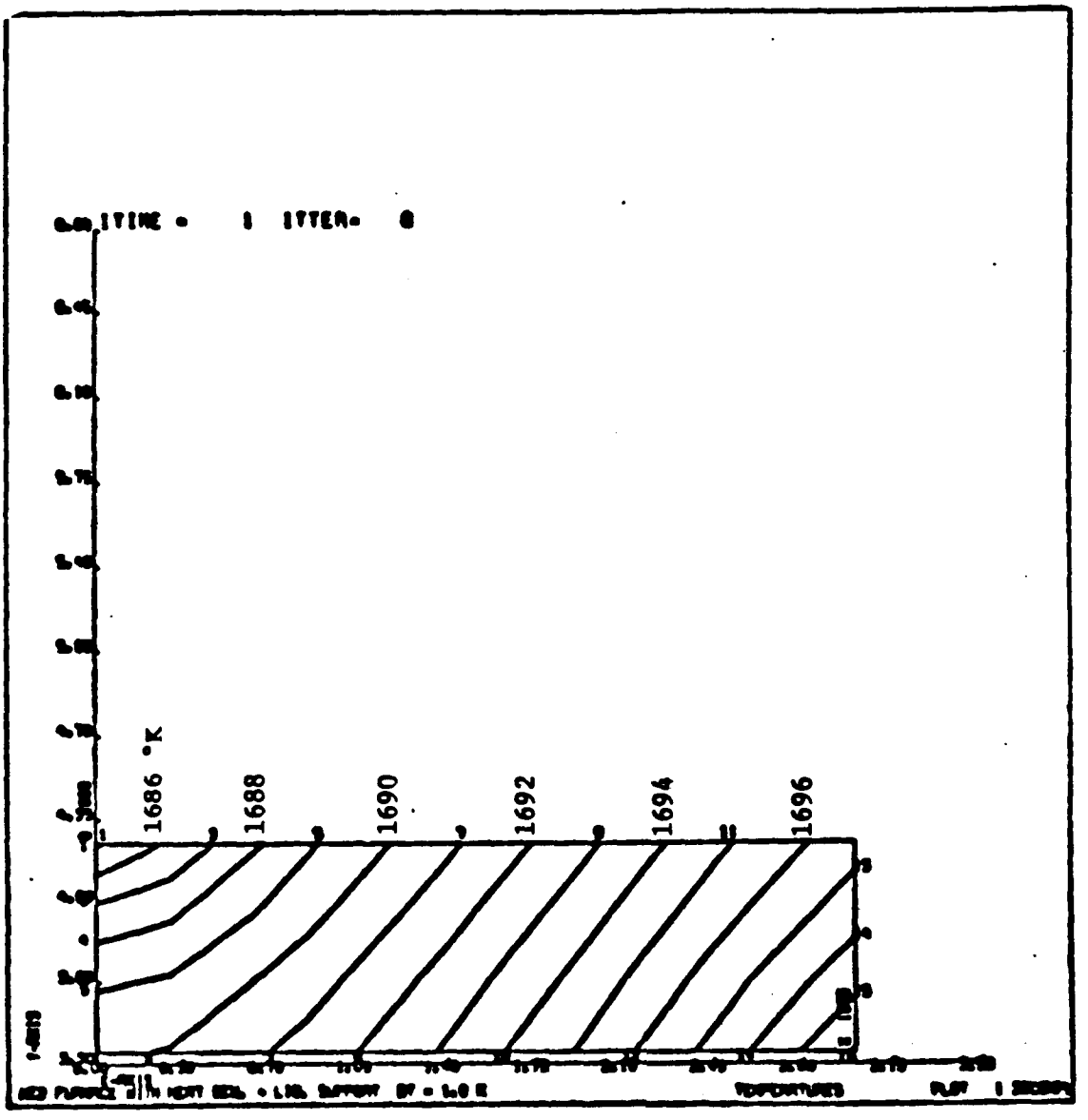

Figure 17. Isotherms in silicon melt resulting from temperature input of Figure 15 when $\varepsilon = 0.3$.

Figure 17. The temperature gradients increased approximately in proportion to the emissivity change. Based on experimental melt temperature data, it appeared that an intermediate emissivity would be more appropriate to the physical situation.

An additional case was run using the two-dimensional model, but changing the power input distribution. In the first two cases, the power input varied along the wall of the susceptor in such a way as to create the specified temperature distribution. In the third case, a uniform power input was assumed along the susceptor wall and adjusted in magnitude to give the proper temperature at the centerline. Some changes occurred in the temperature distribution relative to the first case, but they were less dramatic than those resulting from the change in emissivity.

Finally, a parametric study on the effect of crucible length and temperature on the convective flow in the silicon melt was performed by Profs. Szekely and El-Kaddah. Crucible length is measured in the x-direction of the sketch shown previously in Figure 12. The various cases examined in this study are shown schematically in Figure 18. The first group of cases was formulated to show the effect of the crucible dimensions; the second group was formulated to investigate temperature effects; the third case illustrates the effect of front/back temperature asymmetry in the melt (across the width of the cruible); and the fourth case is a representation of the side-to-side temperature profile in the crucible. The centerlines shown in Figure 18 are the positions where the seed first contacts the molten silicon (theoretically) during the initiation of crystal growth.

The results of these calculations can be summarized as follows:

1. For a given temperature difference between the center and front (or back) of the crucible, the maximum fluid velocity decreases with increasing crucible length.

2. For a given crucible length, the maximum fluid velocity increases with increasing temperature difference.

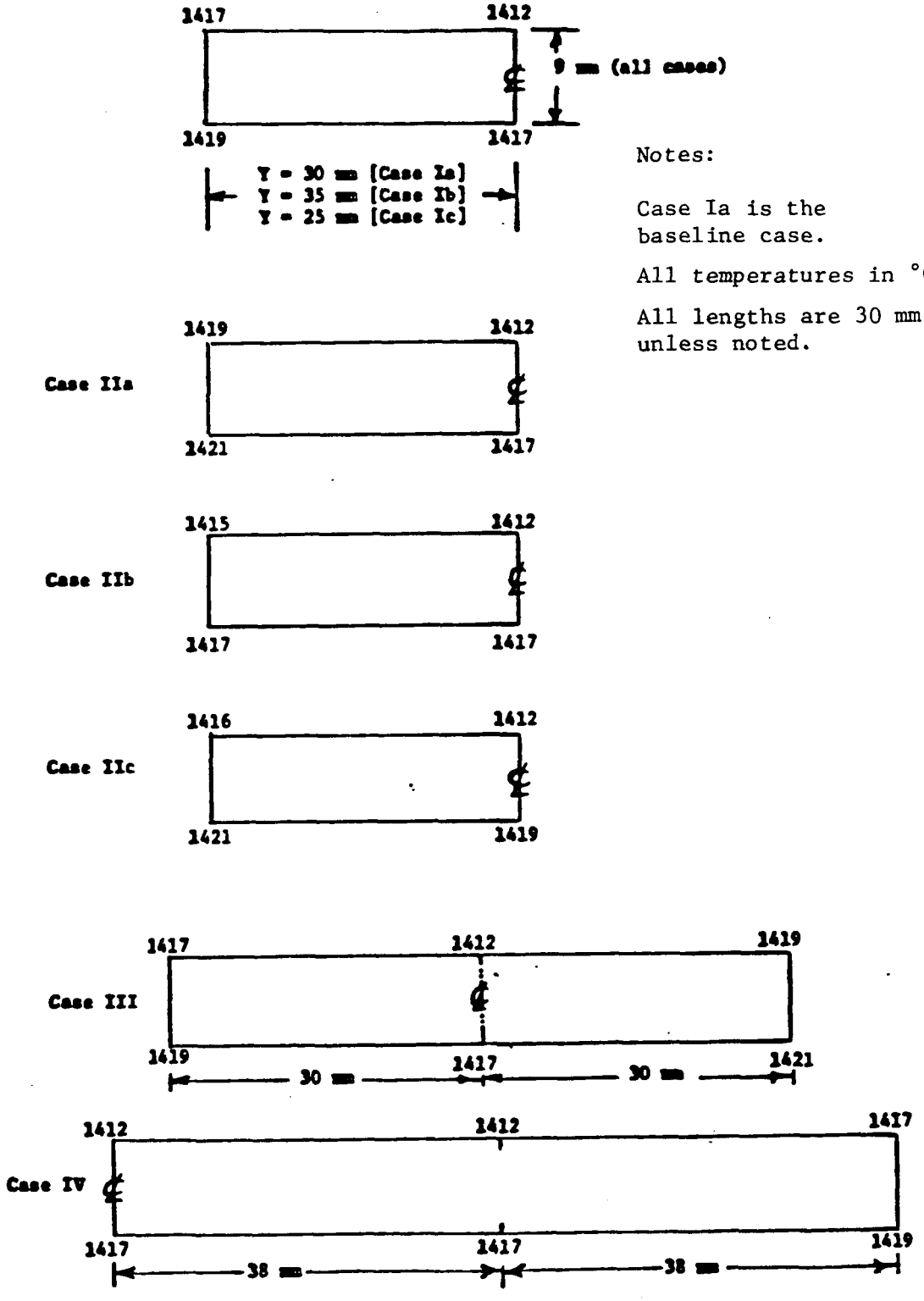

Figure 18. Dimensions and temperatures used for parametric analysis of flow in silicon melt.

These two results can be combined to conclude that the fluid flow depends on the temperature gradient. Furthermore, the results indicate that it is the front-to-back temperature gradient rather than the vertical temperature gradient that dominates convective fluid flow in the molten silicon.

The results in case III, the asymmetric gradient, were of particular interest. The two-degree asymmetry resulted in a shift in the temperature centerline of about 0.7 mm while shifting the center of the flow pattern by about 5 mm. As a result, a web crystal growing in the center of the melt would be only slightly away from the proper thermal position but would be in a location of high fluid flow, where deleterious thermal fluctuations could occur. Thus it is important to obtain a good front-back thermal balance in web growth systems.

In case IV, the approximation to the side-to-side temperature distribution, the results were not so dramatic but still of considerable interest. As would be expected, when the flat temperature profile is induced over the central region of the crucible, there is essentially no lateral flow in this region. This lack of lateral flow gives more veracity to the flow patterns calculated in Cases I through III, since those flow patterns would not be distorted by flow at right angles (in the front-to-back direction in the crucible). Perhaps more interesting, however, was the observation that the lateral flow produced by the lateral temperature gradient extended for a considerable distance into the flat temperature region. This would suggest that flat temperature profiles in a melt should extend well beyond the actual region of web growth to avoid significant flow under the growing tips of the bounding dendrites.

2.3 Web Quality Analysis

The primary goal of the material evaluation activity in the web growth program was to relate the web quality, primarily residual stress and dislocation density distribution, to the growth configuration and

growth conditions. Web structure evaluation techniques are compiled in Table 8. The technique for experimental evaluation of residual stress in a web crystal is depicted in Figure 19.

Table 8. Web Structure Evaluation/Techniques

	PARAMETER	MEASUREMENT TECHNIQUE
1.	Residual Stress	Web Split Width Measurements
2.	Dislocation Density	Etch Pit Counting
3.	Defect Type, Distribution and Structure	X-Ray Topography

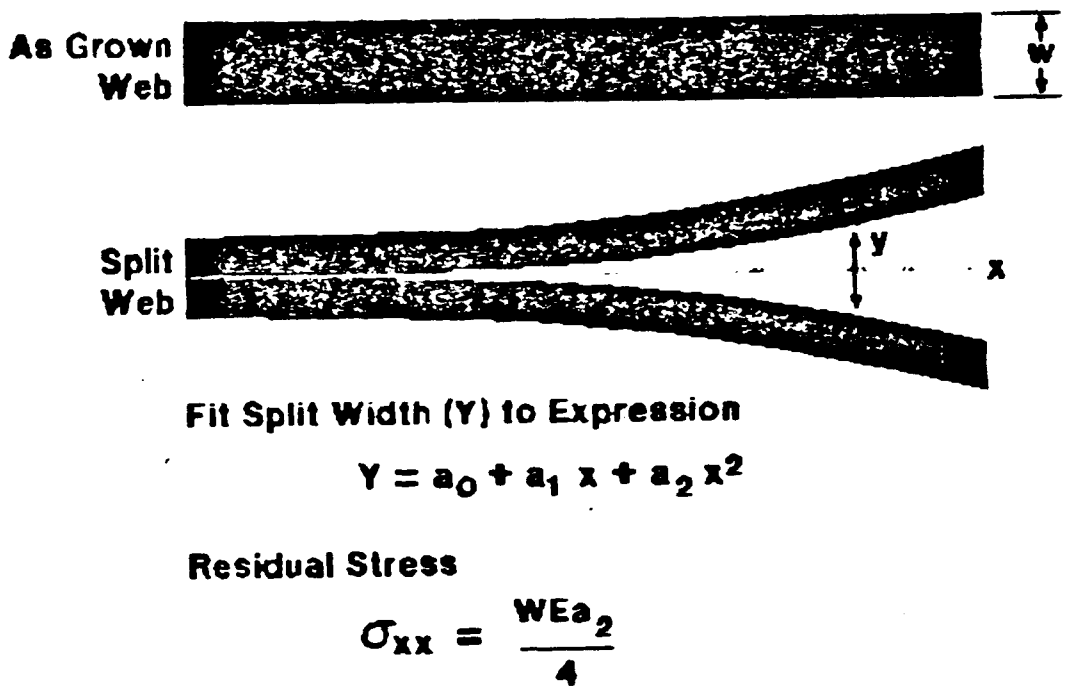

Figure 19. Web residual stress measurement technique.

The initial activity on this task under this contract involved organizing existing etch pit density (EPD) data from crystals grown in the two principal growth configurations being used for production and development: the J435 and the J460L.

Residual stress measurement data for these configurations are presented in Figure 20. Figure 21 presents similar stress measurements along with a comparison of the average etch pit density as a function of position along the length of the web for two crystals, each from the J435 and the J460L configurations. Here it can be seen that in general the EPD for the J435 configuration is four to ten times larger than the EPD for the J460L configuration. Further, the EPD for the J435 material increases along the length of the crystal. In one of the J460L

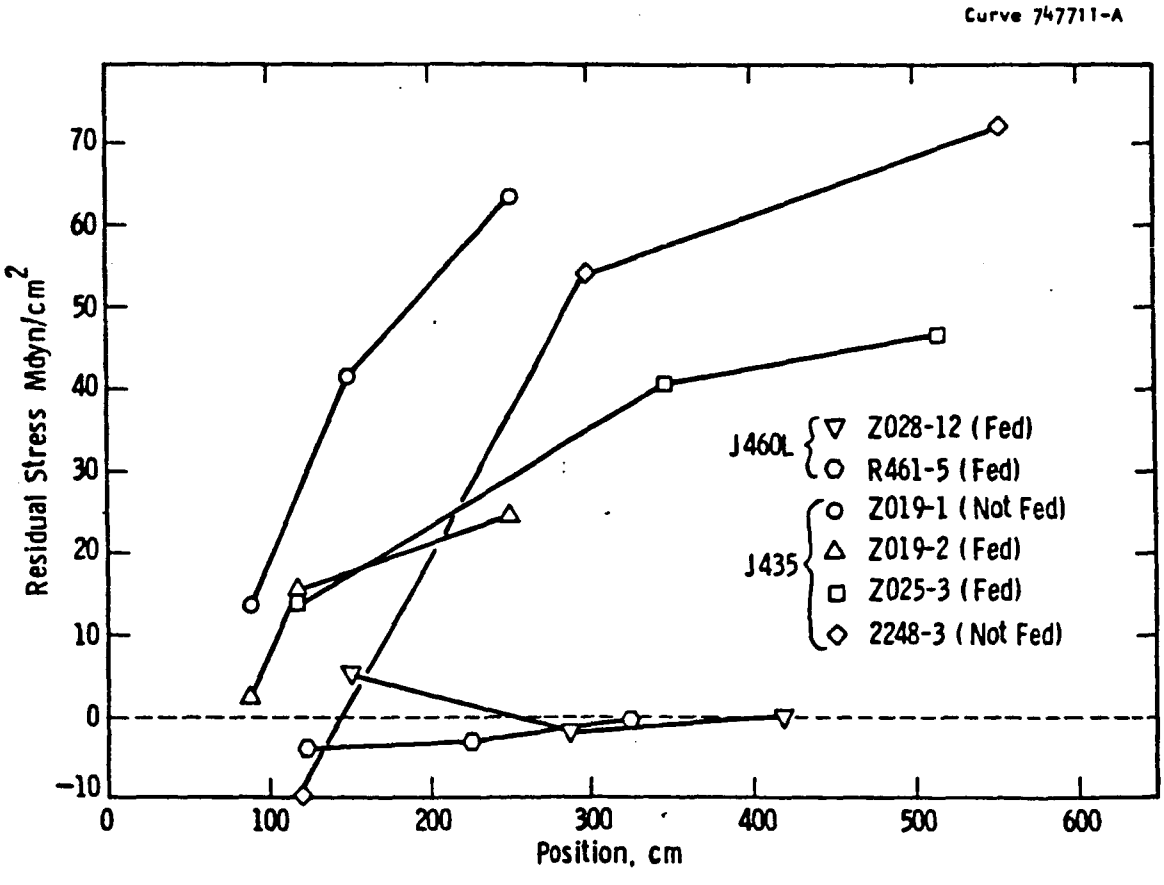

Figure 20. Measured residual stress as a function of length along various crystals grown in J460L and J435 configurations.

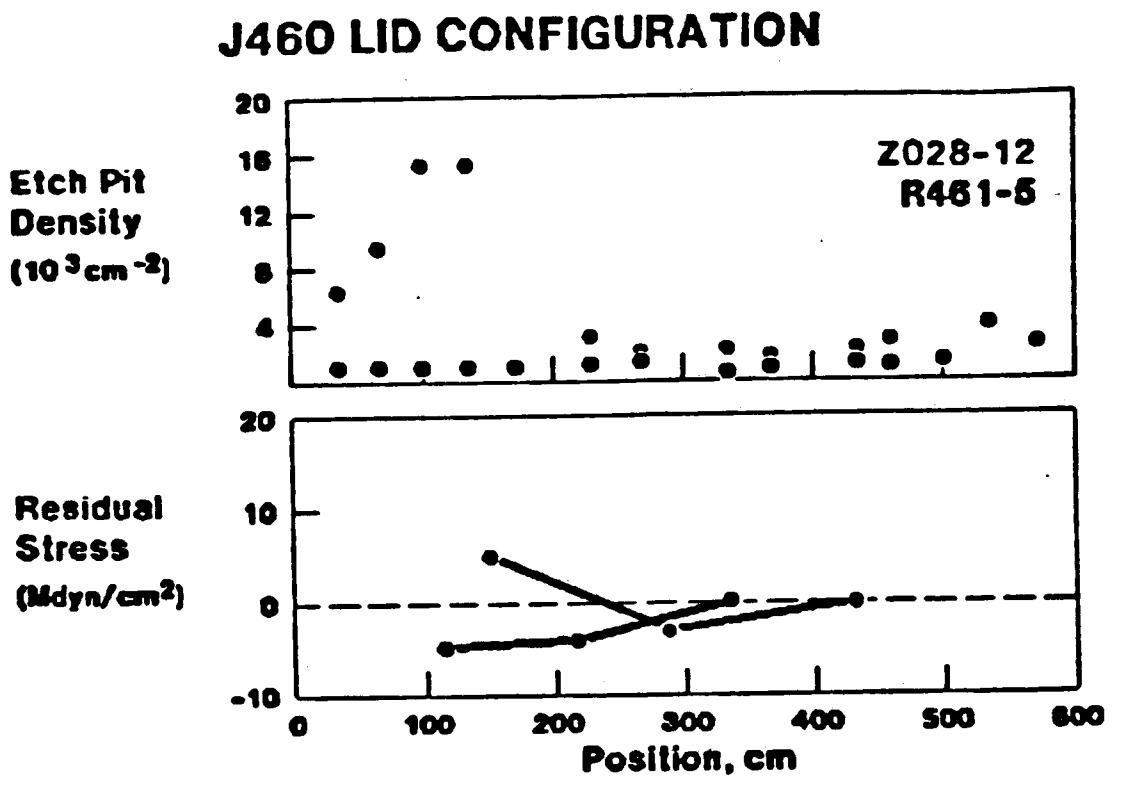

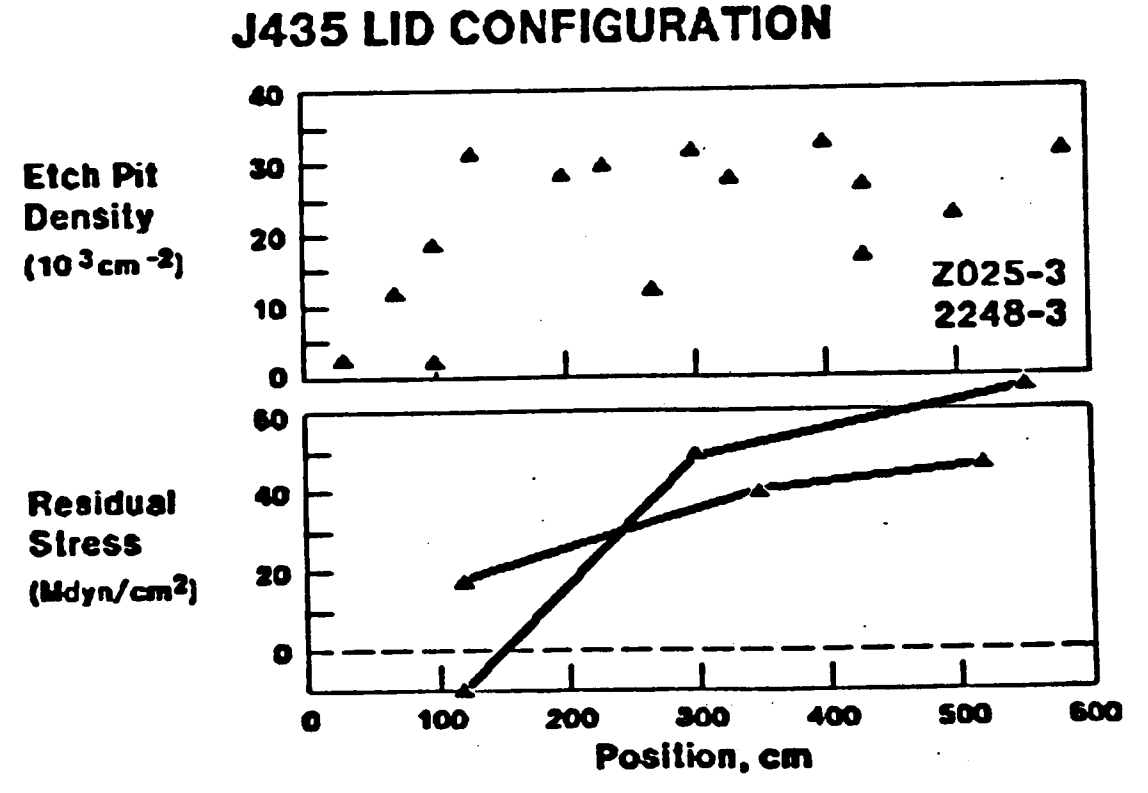

Figure 21. Comparison of etch pit density and residual stress data from two web growth configurations.

crystals, there is an initial peak in the EPD; however, this is followed by a decrease to a relatively constant level.

The relationship between the EPD and the residual stress can be seen from data presented in Figure 21. The increase with length of the EPD for the J435 material is reflected in the residual stress data for the material, although the experimental scatter would make a strictly functional relationship rather vague. In the case of the J460L material, the initial peak of the EPD is echoed by an initial peak in the residual stress value; the relatively small overall value of the EPD is consistent with the small values of the residual stress.

Topographic studies of specimens from this material show that EPD and stress values are generally consistent with the slip systems visible in the specimens. Additionally, there are the typical dislocation lines running along the length of the samples. The effect of these dislocations on stress and on the electrical properties of the material is still not known.

In late September and October of 1984, crystal sampling from the development furnaces was begun on a routine basis. The initial sampling plan used is listed in Table 9. The EPD and stress data collected for the month of October are given in Table 10. It is important to note that the J and R furnaces had long susceptor systems with sloped wall crucibles, while the N and Z furnaces had normal length susceptors with sloped wall crucibles (all susceptors and work coils were rectangular). Also, all the runs were continuously replenished during crystal growth to maintain constant melt level. All the lids and shields were variations of the basic J460 design which were designed to produce low-stress material.

With some exceptions, for example Run R470, the data in Table 10 indicated that the average EPD in the most recent runs was larger than observed in crystals grown from earlier susceptor designs. In addition, the residual stresses were also larger and tended to be negative. Based on these limited initial data, the results tended to indicate that there

Table 9. Crystal Sampling Protocol

Sample Selection:	From all crystals grown greater than 3 m long: a. Button end of crystal b. 33 cm section from end of each succeeding meter c. Any other samples as determined by engineer
Data Requirements:	For samples provided as above, provide: a. Total Crystal Length b. Growth Velocity c. Melt Undercooling d. Melt Height e. Work Coil Settings

had been a change in the temperature distribution in the lids and shields as the result of the use of rectangular susceptors and sloped wall crucibles. Note, however, that the stresses and EPDs were still much smaller than similar data for the J435 crystals.

During the months of October and November of 1984, all the development furnaces were converted to sloped-wall systems of some nature; at the end of the period, only the N furnace had a short susceptor. The focus of the web quality analysis in November was to assess whether these system changes had any significant effects on the quality of the ribbon crystals. Initially, the etch pit densities and stresses for the J460L configuration in the long susceptor system were larger than for the same configuration using the short susceptor. Adjustment of the system temperatures, for example by coil position, brought the residual stress and etch pit densities back to values comparable to the short susceptor cases, e.g., ± 10 Mdyn/cm^2 and less than 6000 pits/cm^2 as shown in Table 11.

A systematic evaluation of etch pit density as a function of ribbon length was made for a number of long crystals grown in either the R or Z furnaces. Prior to adjustment of the system temperature, for

Table 10. Stress and Etch Pit Density Data From Web Grown with J460 Design Variations (October Data)

Run-Crystal-Sample	Etch Pit Density	Stress
J535-1-1	1.2×10^3 cm^{-2}	2.3 Mdyn/cm^2
J535-1-4	5.8	9.5
J535-1-6	10.9	
J535-1-7	114.0	-36.9
J539-1-3	18.4	
J539-2-3	23.9	
J539-8-B	0.55	
J539-8-4	12.5	-0.2
N113-2-A	0.7	
N113-2-5	3.7	-13.0
N117-1-B	6.6	
N117-1-4	12.5	-46.9
Z045-5-5	1.1	-5.7
R468-10-A	0.3	
R468-10-3	5.0	
R469-2-2	5.6	
R469-2-5	1.8	
R470-1-3	0.7	-4.7
R470-4-1	0.6	
R470-4-4	0.9	6.0
R470-4-7	4.6	-9.7
R470-7-1	1.5	
R470-7-5	10.4	
R470-9-5	3.0	2.5

Table 11. Etch Pit Densities and Residual Stress from Web Grown After System Adjustments (November Data)

Run No.	Crystal. Piece No.	EPD $x10^3$	Residual Stress ($Mdyn/cm^2$)
R461	1.3	1.5	
R465	1.B	.825	
	1.3	4.33	-23.41
	1.7	3.79	
R407	3.1	.917	
	3.9	18.6	
	3.11	52.2	
R473	1.3	2.76	
	1.5	8.6	
R473	6.2	3.2	
	6.7	1.11	
	6.11	1.5	
R474	4.D	1.82	
	4.3	.572	8.54
R474	5.1	2.2.	
R474	6.1	4.0	
	6.4	31.9	12.0
R474	8.9		14.7
R474	10.A	.628	
	10.1	.458	
	10.3	.484	
	10.7	.471	7.12
R475	1.1	.275	
	1.6	12.9	1.57
Z047	1.1	4.03	
	1.6	10.9	+44.5
Z048	3.1	4.99	
	3.8	1.44	
	3.14	2.54	
Z049	4.1	1.415	
	4.5	.812	3.09
	4.8	.903	
	4.11	1.073	
	4.14	1.336	
	4.17	.864	15.18
Z049	7.16		7.79
N117	17.2	4.03	
N118	1.1	7.7	-8.48
N119	2.1		43.08
	2.5	5.62	
J539	1.3	18.4	
J539	2.1	4.52	

example in run R-467, etch pit densities exceeded 15,000 pits/cm^2 and increased along the ribbon length. From later runs, for example runs R-470, R-473, R-474, Z-048, and Z-049, etch pit densities are small and essentially constant along the ribbon length (Figure 22). For several of the ribbons, etch pit densities range from only 500 to 1500 pits/cm^2 along many meters of crystals. This suggested that with the proper thermal configuration of the web growth system, long lengths of high-quality web crystals could be grown.

Average stress and etch pit density data measured on crystals grown in sequential runs on the R furnace are presented in Figure 23. These runs were conducted immediately after introducing the long (10") susceptor into the furnace. The data show a temporary increase in defect density initially after the modification, but the defect densities were substantially reduced by incorporating various system adjustments.

2.4 Experimental Web Growth

The objectives of the experimental effort conducted with the developmental furnaces were to investigate high throughput growth using advanced furnace concepts and to demonstrate the ability to grow long crystals while operating in a steady-state replenishment mode.

This task included the modification and development of existing web growth furnaces to attain higher area throughput rates. Also, improved melt replenishment techniques were devised to attain long-term continuous operation. Growth parameters were optimized by conducting tests and analyzing experimental growth characteristics. Figure 24 shows the experimental variations that are addressed for a typical growth configuration.

The initial phase of the experimental growth program was devoted to converting all four developmental furnaces to a rectangular sloped-wall crucible configuration. Work performed under a previous contract indicated that better temperature stability and improved isolation of the growth and replenishment region of the melt are achieved using the

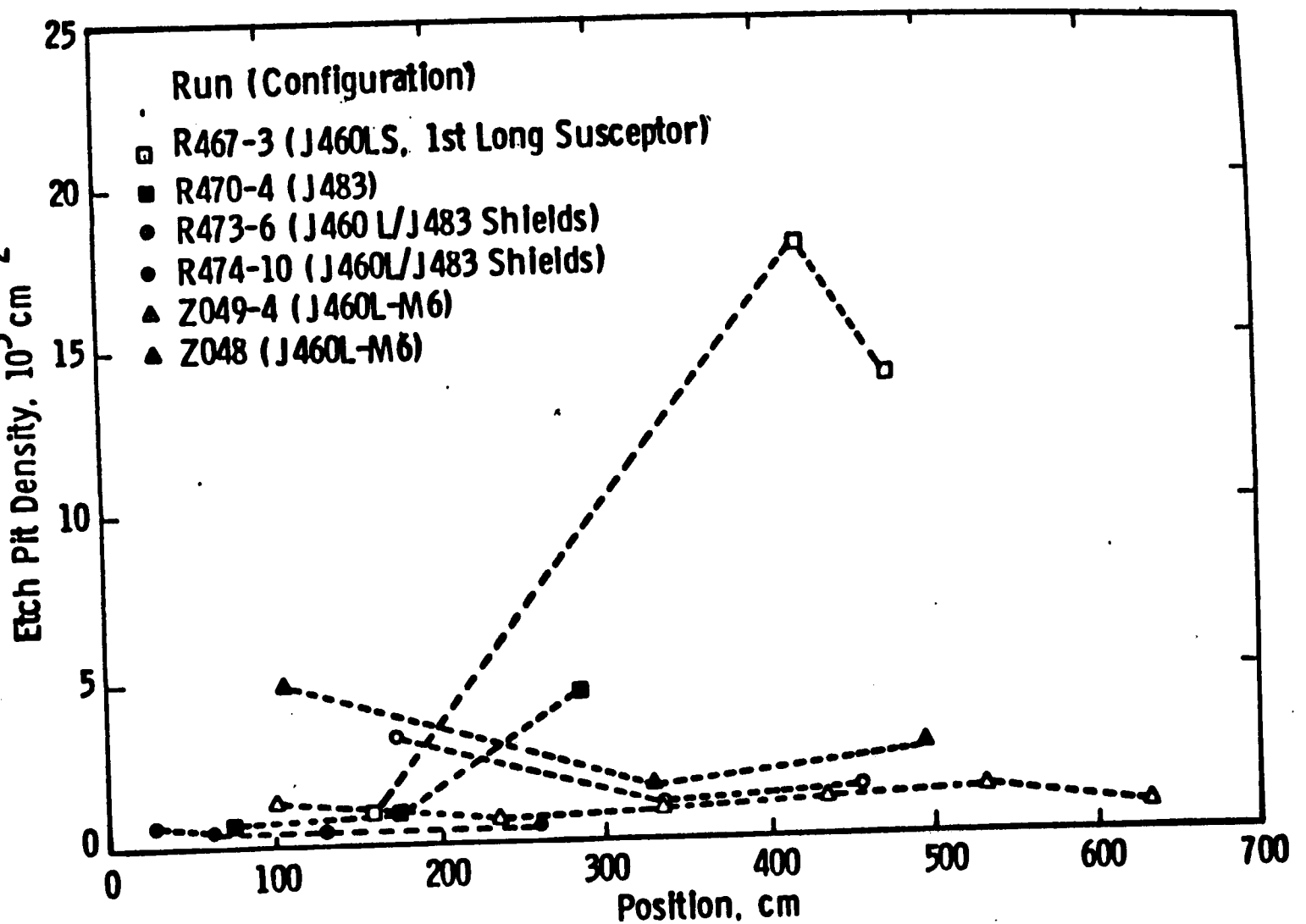

Figure 22. Etch pit density along web crystals.

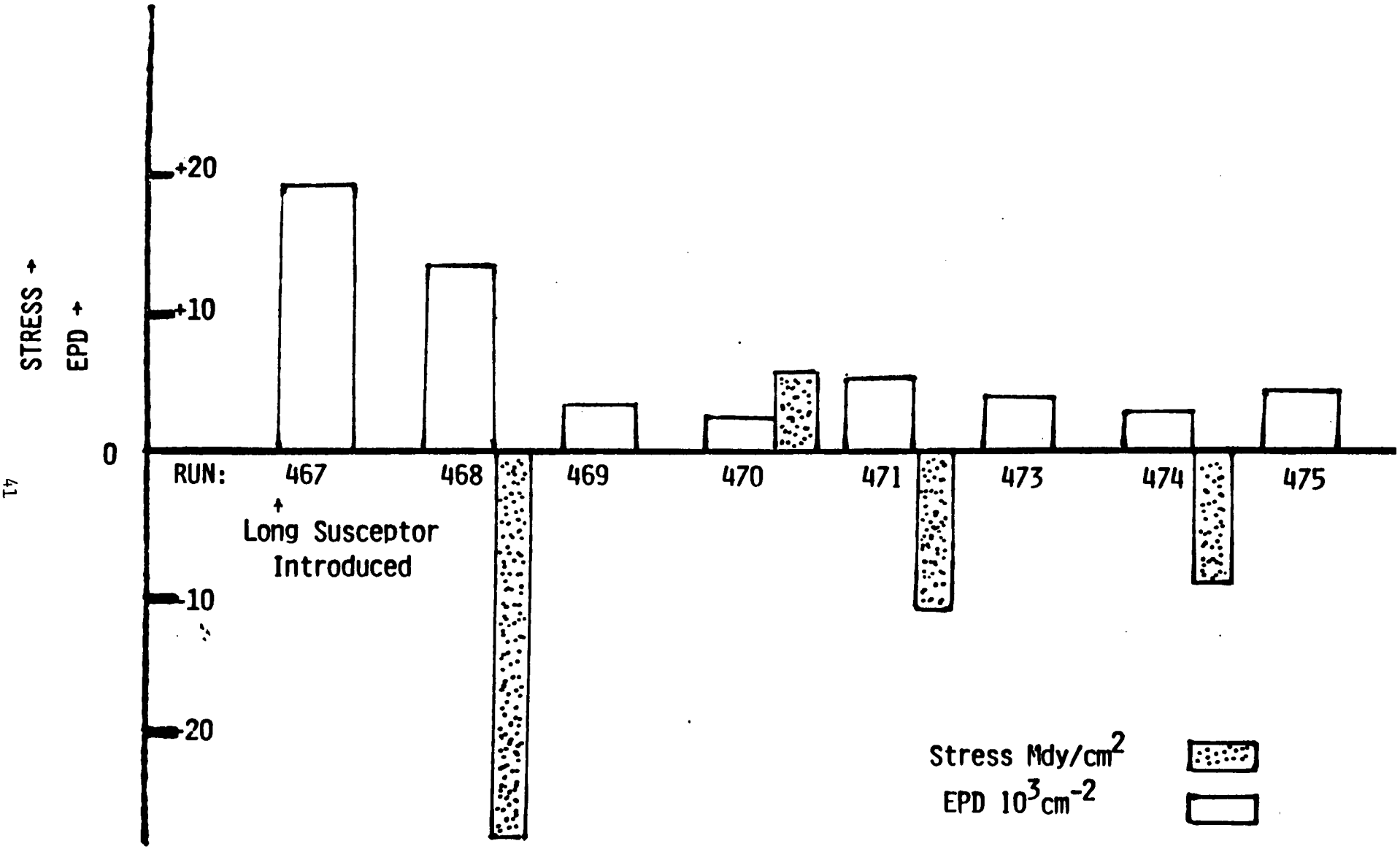

Figure 23. Average stress and etch pit density measured for R-furnace crystals.

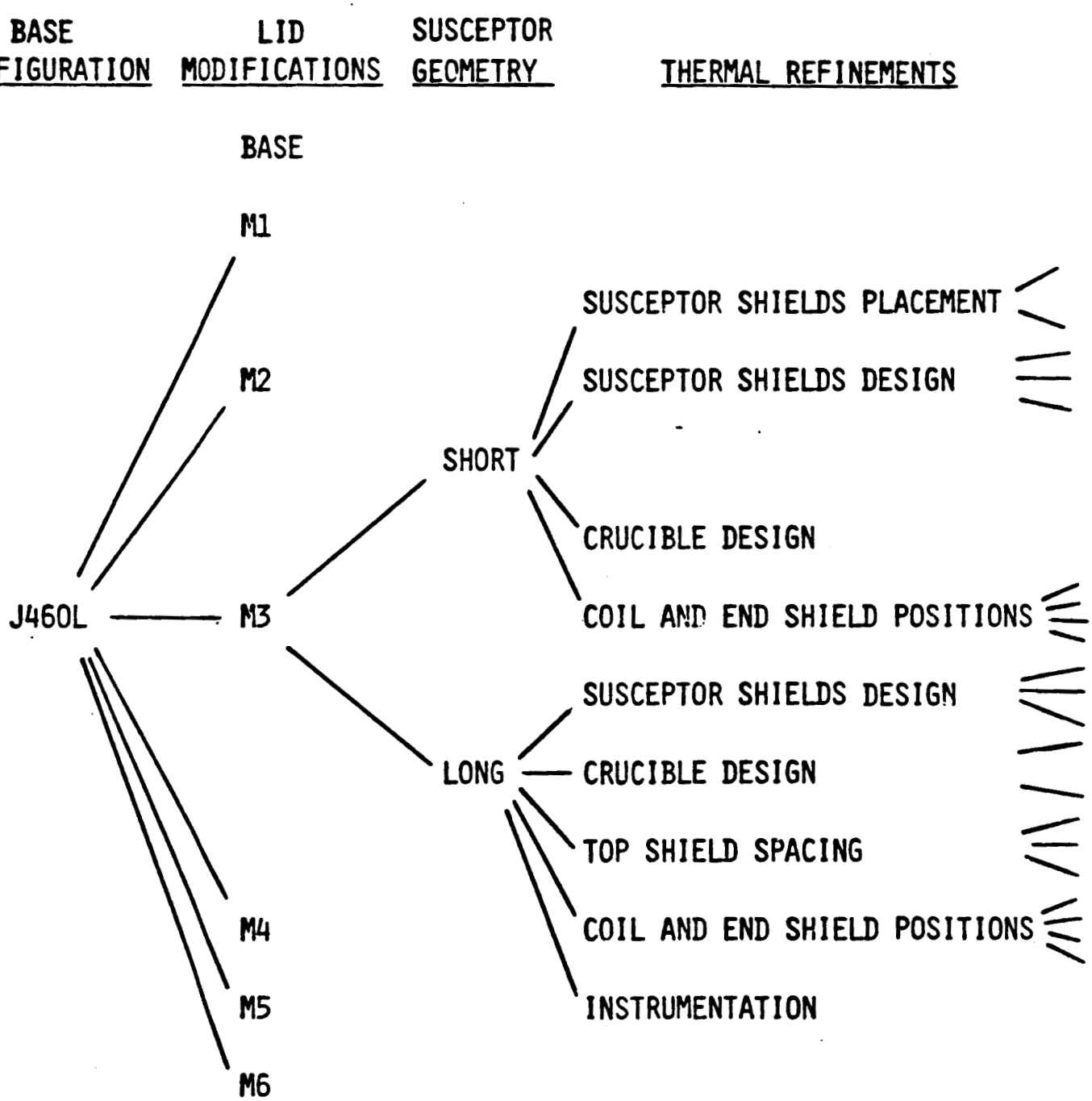

Figure 24. Experimental variations addressed in typical growth hardware modifications.

rectangular sloped-wall configuration. Work performed under this contract verified the improvement.

In September 1984, 16 growth runs were made in the four primary web growth development furnaces, all with continuous melt replenishment. A growth run consists of furnace set-up comprising many crystal starts and lasting up to a full week of operation.

The main effort during September was aimed at obtaining acceptable profiles in the melt for the two sizes of rectangular growth systems. As might be expected, the susceptor shielding requirements were found to be somewhat different from those in the oval growth systems previously used for web growth.

All of the growth configurations used during September were variations of the J460L. Principal variations included changes in the lid growth slot region and in the top shield spacing. These variations were introduced primarily to reduce the y and x stresses in the growing web. In addition, a vertical thermal element was added in one run in the N furnace, yielding some improvement in buckling stress over the baseline configuration, although the results have not yet been fully evaluated.

Systematic run-to-run changes were also made in susceptor shielding to improve the lateral temperature distribution in the melt. Post-run examination showed that in all cases the sloped-wall crucible was in tight contact with the susceptor cavity, so that a significant improvement in the uniformity and reproducibility of heat transfer to the melt was achieved by conversion to the rectangular sloped-wall growth systems.

The first three runs in the R furnace with the new extended growth system produced very encouraging results. A total of 70 meters of crystals over 1 meter long were grown with continuous melt replenishment. Widths reached 4.8 cm. Growth problems attributable to melt replenishment were significantly reduced from previous experience. The purpose of these runs was to systematically move from a J460L

configuration to the lower stress J483L configuration, while making appropriate adjustments in the susceptor shielding to preserve an acceptable temperature distribution in the melt. The lid growth slot was sufficiently wide to allow the crystal to reach a width at which buckling would occur with the J460L configuration. Thus, the chief cause of crystal termination was the onset of stress induced by crystal degradation. Results showed an expected increase in the width at which deformation occurred.

In all but one case, modifications in growth configurations gave the desired results or at least moved in the desired direction. One exception, however, was the J460L-M4 modification, which performed slightly poorer than the baseline J460L in terms of the buckling stresses. A further modification, designated the J460L-M5, was defined as a configuration lying roughly between the baseline J460L and the M4 version.

In October, 17 runs were made in the four development furnaces. Two types of lid configurations were run in the long rectangular configurations, the J460/J483LS designed for 5 cm crystals and the J460L-M3 designed for a 4 cm width limit. Variations in top shield configurations were tested for both lid configurations. Runs with the short rectangular systems were made with the J460L M3 and M5 configurations with some variations in susceptor shielding to improve melt profiles.

One run in the R furnace using the long J460/J483LS configuration with an expanded top shield spacing produced record results: the longest duration of continuous replenishment on a single crystal -- 10.8 hours; the longest replenished crystal -- 6.8 meters; and, up to that time, the largest single-run replenished output -- 36 meters. This run utilized a crucible with double barriers of a new design.

Another run was made in the J furnace using the same lids but incorporating a 2.5 cm vertical element in place of expanded top shield spacing to achieve the desired temperature gradients in the web. This

configuration also seemed to grow well, yielding a 4.7 meter replenished crystal. However, when attempts were made to combine both the expanded shield spacing and the vertical element, a configuration which should produce minimum stress in the web, the oxide deposition changed substantially, prohibiting growth. The convective gas flow patterns seem to be quite sensitive to the design of the vertical shield stack. Based on these results, work was initiated on designs to incorporate the desired web temperature effects, without imposing an unacceptable convective gas flow pattern.

Growth in the short crucible systems was variable. A problem with front-back asymmetry was identified, and this condition was improved by changing the relative front-back heat losses with perforations in the susceptor side shields. Another sporadically encountered problem was welding of the adjustable end shields to the susceptor, so that they were no longer adjustable. Several methods for preventing shield contact with the susceptor were tested, and the most reliable appeared to be the use of ceramic separators at the critical points.

One of the better runs in the N furnace with a J460L M3 configuration yielded 36 meters of crystals, with a maximum replenished crystal length of 5.8 meters.

During the course of this work, some distinct advantages were found with the long rectangular susceptor/crucible geometry. First, acceptable melt temperature profiles and good growth were found to be achievable with the higher stack/lower stress designs generated from the thermal models. Secondly, a significant improvement in decoupling between growth and replenishment effects was achieved. Thus, it was found easier to concentrate on those parameters that directly affect the quality of crystal growth. For these reasons, installation of a third elongated growth system was initiated in the Z furnace.

In November, the Z furnace was converted to the long rectangular sloped-wall growth configuration. A new lid design was fabricated for

use in this system. The design, designated the J460LS-M6, is the same as the J460 in the vertical direction but incorporates a slot geometry aimed at a crystal width limited to 3.3 cm, well below the buckling stress limits for the J460 design. The rationale for this design is to grow long crystals at higher growth velocities.

During the first run, crystal lengths of 4.6 and 5.4 meters were achieved. In the next run, a new record replenished crystal, 7.06 meters in length, was grown. In addition, a 2.9 meter long crystal was grown at a growth velocity of 2.1 cm/min.

The performance of this growth system was sufficiently encouraging that conversion of the N furnace to a long rectangular susceptor with lids and shields to duplicate the Z furnace configuration was initiated.

The R furnace was run in November with the J460LS-M3 configuration, aimed at 4 cm crystal widths. The maximum crystal length was only 5.4 meters. Some effort was directed toward improving growth velocity by testing growth at various accurately measured melt levels and coil elevations. A number of crystals were grown at 1.5 to 1.6 cm/min, below the predicted capabilities of the growth geometry but still an improvement over past averages.

A new cover plate was installed on the J furnace. The new cover incorporates a wider chimney, laser ports positioned to allow melt level sensing in the long susceptor, repositioned end-shield positioning rods to permit unencumbered measurement of dendrite edge thickness, provision for improved susceptor temperature measurements, and provision for covering view ports to reduce oxide accumulation. Modified electronics for the melt level control system were also installed. The hardware for the new laser mounting was received, and installation was initiated.

Results of thermal modeling, discussed in Section 2.1 of this report, indicated that the J460 growth configuration is capable of growing web with sufficiently low buckling stresses to sustain growth at widths in excess of 5 cm and at speeds up to 2 cm/min. This combination yields area throughput greater than 10 cm^2/min. These thermal models

address temperature distributions in the growing web, but melt temperature distributions must satisfy the requirements for growth before the potential of any furnace configuration can be met.

Figure 25 is a plot of long crystals (longer than 4 meters) grown in the replenishment mode in a nine-month period during 1984. No crystals longer than four meters were grown in this mode prior to this time. The plot shows the increasing frequency of long crystals since the introduction of the long (10") rectangular sloped-wall system.

Figure 26 is a pie-chart that identifies the types of terminations associated with the long crystals. The average growth time for these crystals ranging in length from 4 to 7 meters was 7.1 hours and the maximum was 11 hours. From this data it is obvious that melt replenishment problems have been significantly reduced through the introduction of the long rectangular, sloped-wall growth system.

Figure 27 addresses "effective" growth velocities in developmental furnaces along with representative data from the pre-pilot line furnaces using the standard J435 configuration with no replenishment. Effective growth velocity is defined as the ratio of the total length of crystals grown in a given growth run to the total time that the furnace was held at operating temperature. A typical growth run lasts approximately one week.

The data show that despite the experimental nature of the developmental growth runs, the effective growth velocity is nearly twice that of the standard pre-pilot line furnaces. The primary reasons for the low effective velocity in the pre-pilot line furnaces is the lost growth time involved with manually replenishing silicon between crystals and the necessity for gradually reducing the growth velocity as the unreplenished melt level falls.

Table 12 summarizes the equipment modifications made to experimental growth furnaces during the course of this three-month program. Table 13 summarizes the lid and shield configuration variations investigated on the contract to improve stress and growth characteristics.

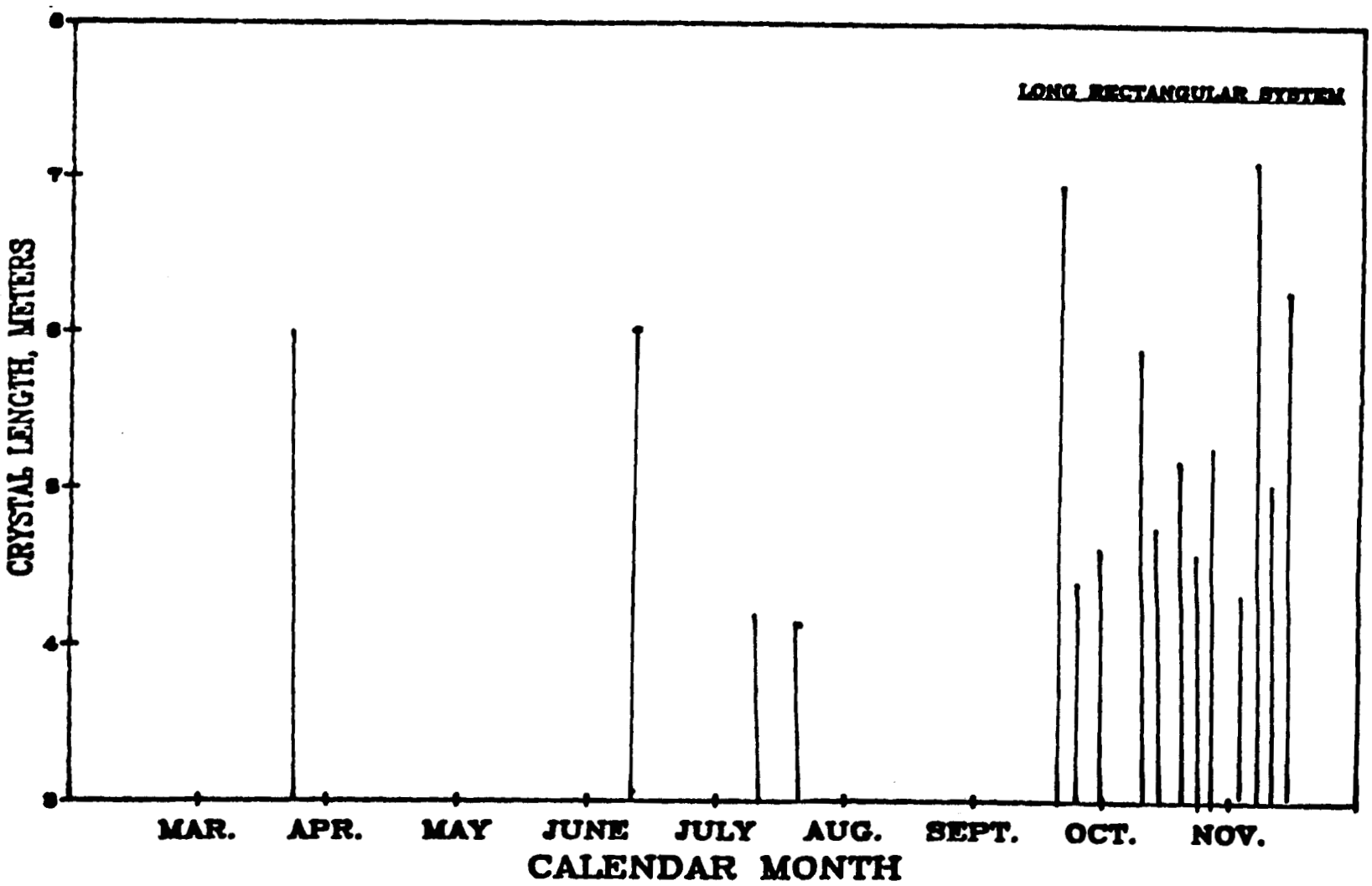

Figure 25. Record of crystals grown longer than 4 meters during replenishment.

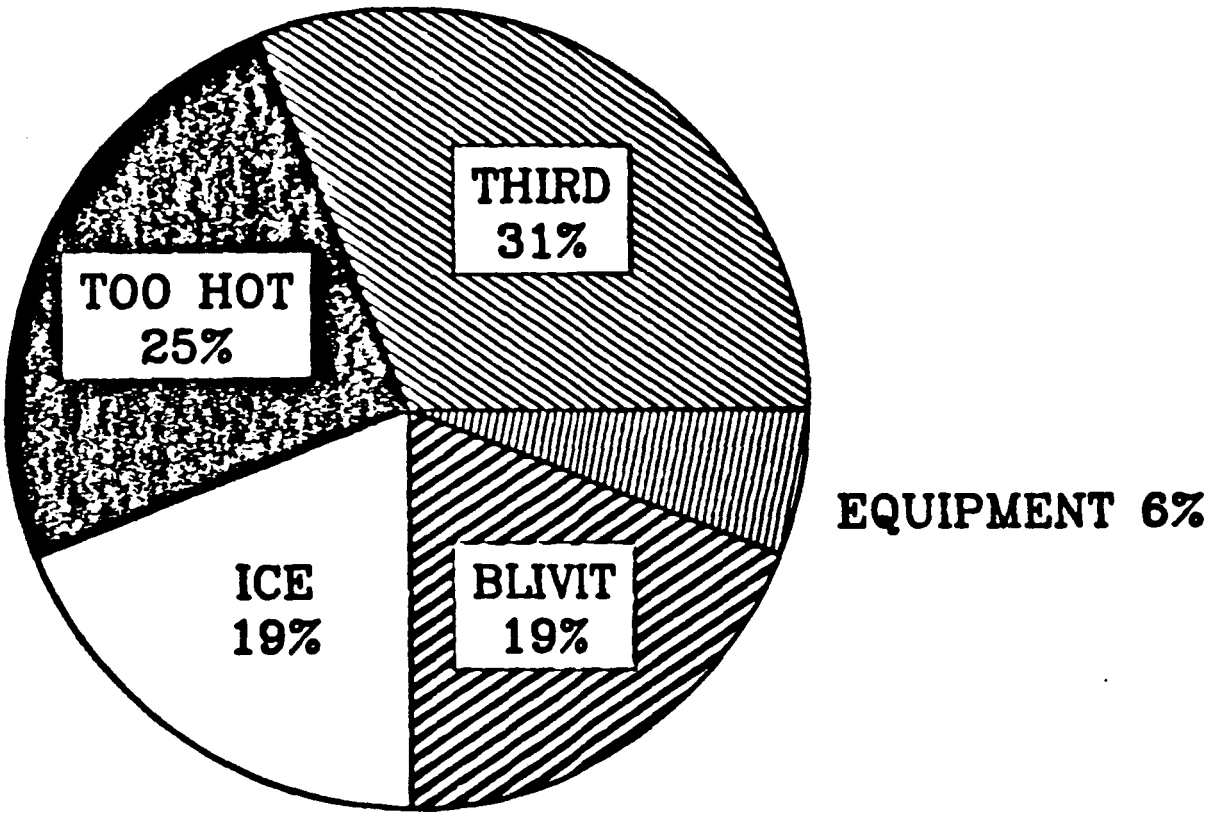

Figure 26. Causes for termination of long crystals.

Figure 28 shows the improvements made in terms of crystal length and replenished growth time since the initiation of work described in this report. Maximum crystal lengths have more than tripled, and growth times have increased by nearly a factor of four. Despite this progress, however, the 10 meter long crystal goal has not yet been reached. A primary factor in the lower than anticipated crystal lengths was the fact that growth speed improvements did not keep pace with growth stability improvements. It has been observed that the switch to the long crucible configuration that produced the improved growth stability (better temperature distribution in the molten silicon) had an adverse effect on axial temperature distribution along the length of the grown crystal; this produced higher stresses in the growing ribbons. To compensate for the increased stresses, it was found necessary to grow thicker web, hence lower pull speeds were used.

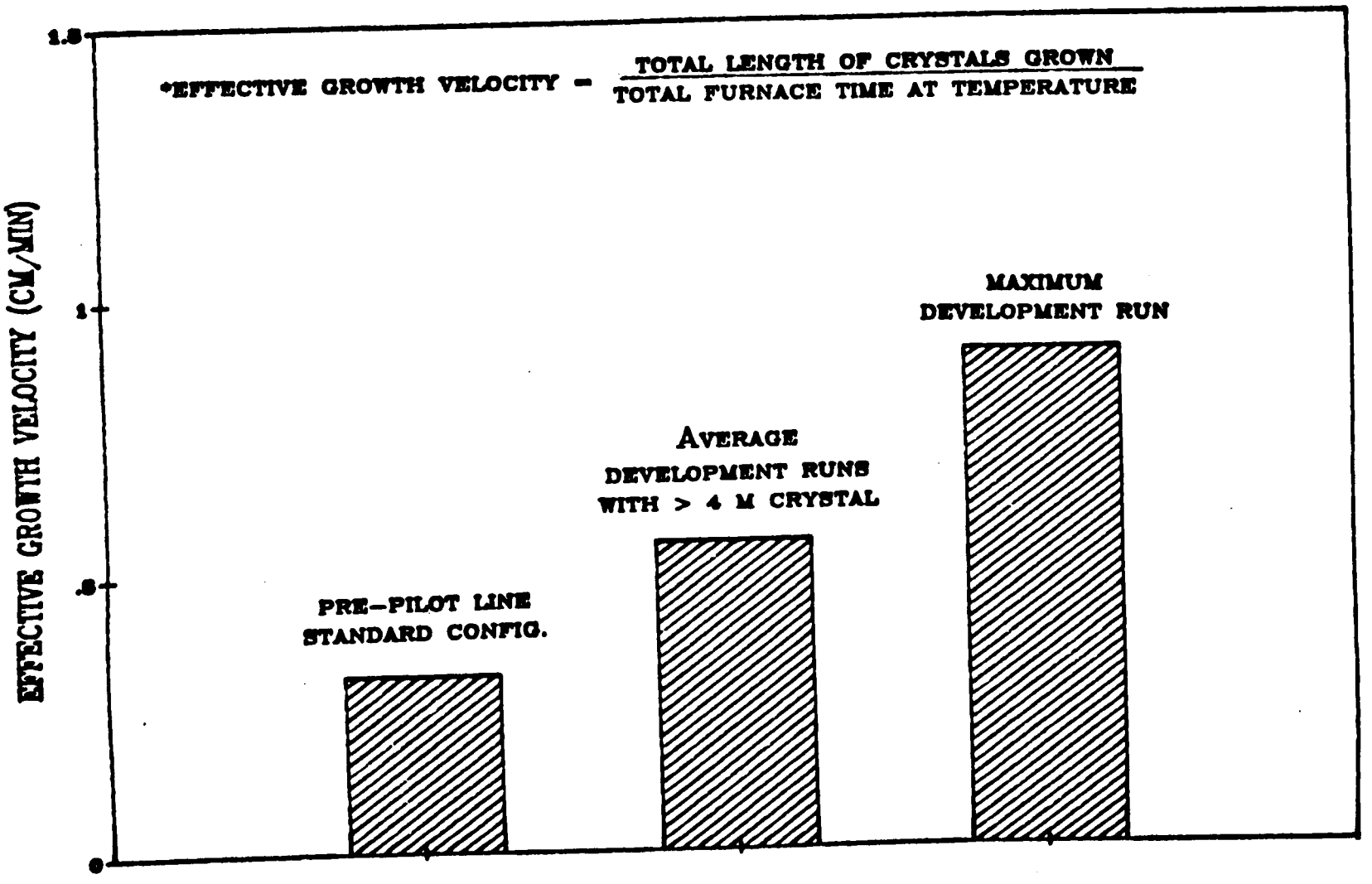

Figure 27. Effective growth velocities for pre-pilot line and experimental growth furnaces.

Table 12. Major Equipment Modifications

- Z furnace converted to long rectangular growth system in November
- N furnace converted to long rectangular growth system in December
- New top cover installed on J furnace with the following features:
  1. Wider chimney
  2. Laser ports matched to long susceptor
  3. Allows for dendrite thickness monitoring
  4. Provisions for covering view ports
  5. Provisions for more temperature measurements
- Laser melt sensing hardware installed on J furnace
- Feeder with commercial pellet material installed on R furnace
- Larger susceptor concepts identified
  1. Material requirements identified and procurement initiated
  2. Equipment requirements identified and procurement initiated

Table 13. J460L Type Lid and Shield Configurations

Designation	Design Function
J460L	Low Stress Web at Controlled Width of ~4 cm
J460L-M1	Low Stress Web at Controlled Width of ~3.8 cm
J460L-M2	Alter Temperature Distribution in Y-Direction
J460L-M3	Alter Temperature Distribution in Y-Direction
J460L-M4	Rectangular Version of J460L-M2
J460L-M5	Modification of J460L-M2
J460LS	Stretched Version of J460L, 5 cm Wide Web
J460LS-M3	Long System, M3 Lids
J460/483 LS	Long System, J483 Top Shield Stack
J460LS M6	Long System, Controlled Width of 3.3 cm

NOTES: 1. Mx designates lid slot modification
2. S = Long Growth System = 10 Inch Crucible

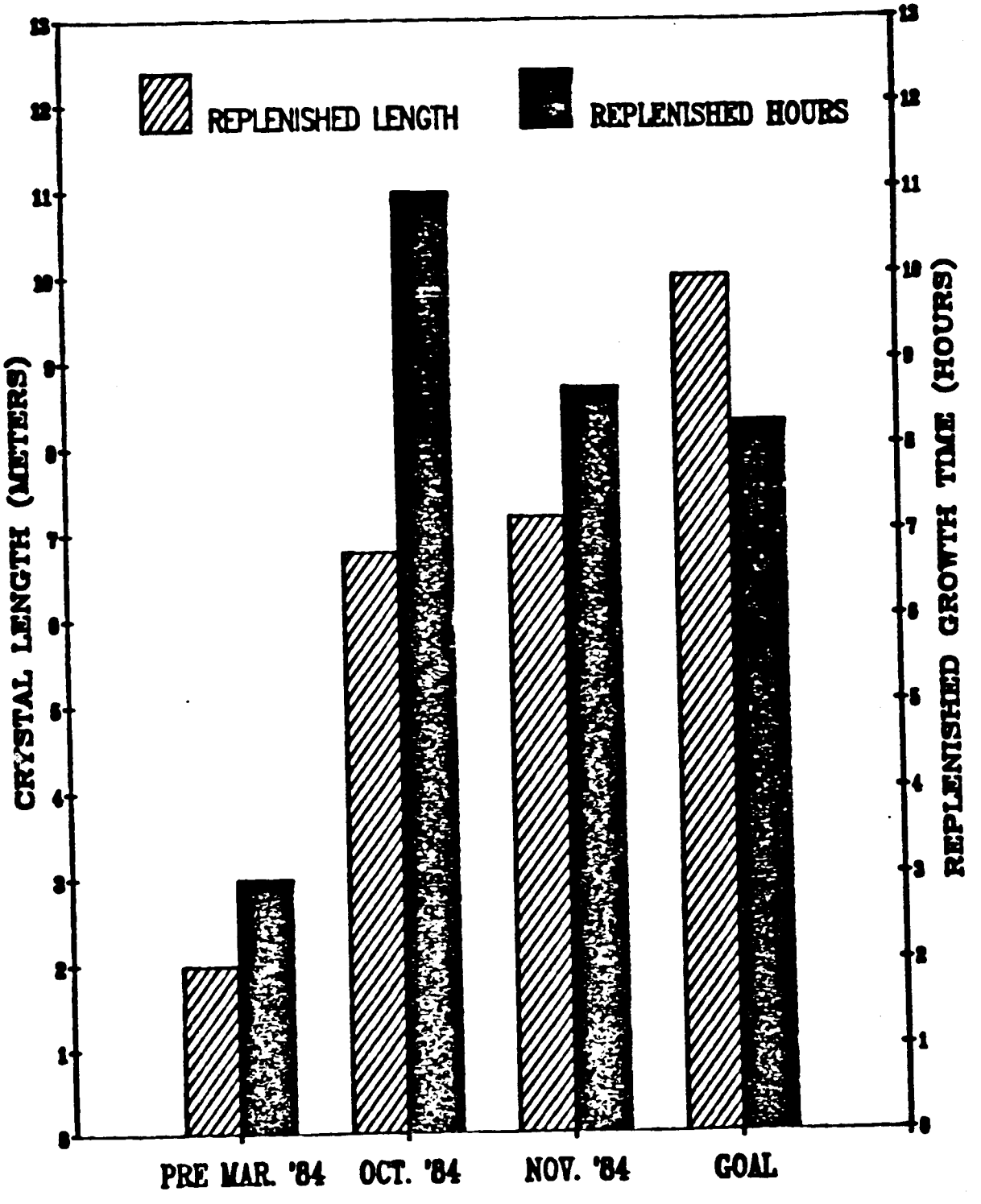

Figure 28. Progress (crystal length and time) made toward 1984 growth objectives.

3. RECOMMENDATIONS

Work performed on this contract has led to a significantly improved understanding of the parameters controlling the rate at which dendritic web silicon ribbon crystals can be grown. Realizing the improvements required to demonstrate commercial technical readiness of dendritic web growth requires additional effort in all areas covered by this contract. The substance of the recommended effort is described in this section of the report.

3.1 Stress Modeling

Computer modeling must be conducted to define growth configurations capable of production of high-quality ribbon (having suitable thickness and low stress) at increased area growth rate and under conditions of continuous melt replenishment. "Continuous melt replenishment" is defined as the condition in which the silicon melt is being replenished at the same rate that it is being consumed by ribbon growth, providing constant melt level (CML) conditions.

The computer modeling should be directed at assessing web stress tendency of the web to buckle near the top of the shield stack (far stress) and plastic stresses generated very near to the growth interface (near stress).

Modeling of stresses generated in growing web crystals near the crystal-liquid interface (near stress) should be performed to characterize and minimize plastic flow and plastic-elastic stress interactions. The coupling of in-plane plastic deformation, elastic and plastic buckling, and resulting web termination modes should also be investigated. This effort should include an assessment of available high-temperature mechanical property data, allowing expansion of the

existing WECAN model to include elastic anisotropy of silicon and yield stress criteria.

3.2 Fluid Flow Modeling

A study of the effects of convection in the molten silicon must be conducted to achieve the improved growth stability required for high speed growth. Both two- and three-dimensional analyses of the thermal environment and convective flow in the melt are required. Susceptor modifications to reduce temperature gradients producing convection should be assessed. For example, the effectiveness of incorporating baffles in the crucible to inhibit melt convective currents should be evaluated. Finally, an analysis of the potential for magnetic stabilization of the molten silicon against convection should be made.

3.3 Web Quality Analysis

Planar and cross-section specimens of web using Transmission Electron Microscopy (TEM) should be examined to assess possible correlations of (111) surface etch features with the internal defect structure induced by deformation under web growth conditions. Growth-induced stresses must be related to both fine and large-scale defect structures which can degrade the web and minimize conditions that favor deformation.

Features such as slip traces and location of contaminants (SiO_2, metals, etc.) that may result from gas phase interactions should be correlated with growth configurations. Techniques for minimizing those defects that adversely affect cell performance and influence plastic flow must be identified.

3.4 Closed Loop Furnace Operation

A closed loop control system must be devised and developed to allow long-term, stable, constant melt level growth of dendritic web crystals. This system must control the (1) average melt temperature,

(2) left-right melt thermal symmetry, and (3) melt level to provide steady state growth (no terminations due to pull-outs or extra dendrites). The system must maintain constant melt level either with an active laser-sensor control and silicon pellet feeder or by fixing the feed rate of a calibrated pellet feeder to exactly match the silicon consumption during crystal growth. In conjunction with this effort, alternate methods for pellet feeding, sensing of pellet drops (uniform dispensing), and improved crucibles and lid configurations to maintain thermal symmetry while feeding should be pursued. Alternate pellet-feeding methods investigated should include vibratory techniques. Acoustic and photoelectric sensors should be investigated to detect and count pellet drops.

Flat Plate Solar Array Project

Contractor Quarterly, Annual, Interim, and Final
Report Distribution List

Acurex Corporation 1
Attn: W. Z. Masters
485 Clyde Ave.
Mt. View, CA 94042

Aerospace Corporation 1
Attn: Dr. Stanley L. Leonard
P. O. Box 92957
Los Angeles, CA 90009

Aerospace Corpration 1
Attn: Mr. Howard Weiner
Building A2 M/S 2037
P. O. Box 92957
Los Angeles, CA 90009

Alcoa 1
Attn: Mr. Gregory Barthold
1200 Ring Bldg.
Washington, DC 20036

AMP Incorporated 1
Attn: Edward J. Whiteman
Mail Stop 39-11
P. O. Box 3608
Harrisburg, PA 17105

Amperex, Inc. 1
Attn: J. Dowdle
3760 Cahuenga
No. Hollywood, CA 91604

Applied Solar Energy Corporation 1
Attn: D. C. Leung
15251 East Don Julian Road
City of Industry, CA 92634

Arco Solar, Industries 1
Attn: James C. Arnett
P. O. Box 4400
Woodland Hills, CA 91365

Arco Solar, Inc. 1
Attn: Library/Aggie Raeder
P. O. Box 4400
Woodland Hills, CA 91365

Arizona State University 1
College of Engr. Science
Attn: Dr. Charles E. Backus
Tempe, AZ 85281

Dr. D. L. Bailey 1
627 West Ninth Street
Traverse City, MI 49684

Battelle Memorial Institute 1
Columbus Laboratory
Attn: Dr. Donald C. Carmichael
505 King Ave.
Columbus, OH 43201

Battelle Memorial Institute 1
Columbus Laboratory
Attn: G. Gaines
505 King Avenue
Columbus, OH 43201

The BDM Corporation 1
Attn: Mr. J. Scott Hauger
7915 Jones Branch Drive
McLean, VA 22101

Bell Aerospace Textron 1
Attn: Frank M. Anthony
P. O. Box 1
Buffalo, NY 14240

The Boeing Company 1
Attn: Elizabeth Zimmerman
M/S 88-05
P. O. Box 3999
Seattle, WA 98124

Brown University 1
Dept. of Engineering
Attn: Dr. Joseph J. Loferski
Providence, RI 02912

Burt Hill Kosar Rittelmann Assoc. 1
Attn: John Oster Jr.
400 Morgan Center
Butler, PA 16001

Carnegie-Mellon University 1
Dept. Electrical Engineering
Attn: Dr. Art Milnes
Schenley Park
Pittsburgh, PA 15213

Central Solar Energy Research Corp. 1
Attn: Dr. W. Lance Haworth, Ph. D.
328 Executive Plaza
1200 Sixth Street
Detroit, MI 48226

Clarkson College of Technology 1
Dept. of Chemical Engineering
Attn: W. R. Wilcox
Potsdam, NY 13676

Clemson University 1
Dept. of Elect. & Computer Engr.
Attn: Proffessor J. W. Lathrop
Clemson, SC 29631

Colorado State University 1
Attn: Prof. W. S. Duff
Ft. Collins, CO 80521

Comsat General Corporation 1
Attn: Dr. Denis Curtin
950 L'Enfant Plaza SW
Washington, DC 20024

Comsat Laboratories 1
Attn: John Lyons
22300 Comsat Drive
Clarksburg, MD 20734

Crystal Systems, Inc. 1
Attn: Frederick Schmid
Shetland Industrial Park
35 Congress St.
Salem, MA 01970

Hemlock Semiconductor Corporation 1
Attn: G. McCormick
Mail Stop #092
Midland, MI 48604

Eagle Pitcher Industries, Inc. 1
Attn: Mr. Paul Grayson
P. O. Box 1090
Miami, OK 74354

Eaton Corp. 1
Semiconductor Equip. Oper.
Nova Implantation Dept.
Attn: Allen R. Kirkpatrick
16 Tozer Road
Beverly, MA 01915

Electric Power Research Institute 1
Attn: Dr. Edward Demro
3412 Hillview Avenue
P. O. Box 10412
Palo Alto, CA 94304

Energy Materials Corporation 1
Attn: Dave Jewett
Ayer Road
Havard, MA 01451

Exxon Research & Engineering Co. 1
Attn: Dr. James Amick
P. O. Box 8
Linden, NJ 07036

John D. Furber, Jr. 1
1717 18 Street NW
Washington, D. C. 20009

General Electric Company 1
Attn: R. N. Hall
Corp. R & D
P. O. Box 43
Schenectady, NY 12301

General Electric Company 1
Valley Forge Space Center
Attn: G. J. Rayl
Room M2445
P. O. Box 8555
Philadelphia, PA 19101

Grumman Aerospace Corporation 1
Attn: Mike Russak
Plant 26
Bethpage, NY 11714

Honeywell, Inc. 1
Corporate Technology Center
Attn: J. D. Heaps
10701 Lyndale Avenue South
Bloomington, MN 55420

Hughes Aircraft Company. 1
Attn: E. L. Ralph, S1ZV330
P. O. Box 92919
Los Angeles, CA 90009

ICT, Inc. 1
Attn: L. P. Kelley
1330 Industrial Drive
Shelby, MI 49455

IIT Research Institute 1
Attn: John E. Gilligan
10 West 35 Street
Chicago, IL 60616

Institute of Energy Conversion 1
University of Delaware
Attn: John D. Meakin
One Pike Creek Center
Wilmington, DE 19808

International Rectifier 1
Semiconductor Division
Attn: M. F. Gift
233 Kansas Street
El Segundo, CA 90245

Jet Propulsion Laboratory 1
Attn: (Contract Negotiator)
M/S 511-303
4800 Oak Grove Drive
Pasadena, CA 91109

Jet Propulsion Laboratory 35
Attn: Solar Data Library
M/S 502-414
4800 Oak Grove Drive
Pasadena, CA 91109

Jet Propulsion Laboratory 1
Attn: (Secretary)
M/S 512-103
4800 Oak Grove Drive
Pasadena, CA 91109

Jet Propulsion Laboratory 1
Technology Utilization
Attn: L. P. Speck
M/S 180-302
4800 Oak Grove Drive
Pasadena, CA 91109

Kayex Corporation 1
Hamco Division
Attn: R. L. Lane
1000 Millstead Way
Rochester, NY 14624

Kulicke & Soffa Industries, Inc. 1
Attn: Max Bycer
507 Prudential Road
Horsham, PA 19044

Lamar University 1
Attn: Dr. Carl L. Yaws
P. O. Box 10053
Beaumont, TX 77710

Arthur D. Little, Inc. 1
Attn: Dr. David Almgren
Room 20-531
Acorn Park
Cambridge, MA 02140

Lockheed Missiles & Space Co. 1
Attn: L. G. Chidister
Dept. 62-25, Bldg. 151
P. O. Box 504
Sunnyvale, CA 94088

Los Alamos Scientific Laboratory 1
Attn: S. W. Moore
Group Q-11, Mail Stop 571
Los Alamos, NM 87545

Materials Research, Inc. 1
Attn: Dr. Ram Natesh
790 East 700 South
Centerville, UT 84014

McDonnell Douglas 1
Astronautics Co-East
Materials & Processes
Attn: Mr. L. G. Harmon
Bldg. 106/4/E7
St. Louis, MO 63166

Mobil Solar Energy Corp. 1
Attn: K. V. Ravi
16 Hickory Drive
Waltham, MA 02154

Mobil Solar Energy Corp. 1
Attn: F. V. Wald
16 Hickory Drive
Waltham, MA 02154

Monegon, Ltd. 1
Attn: Scott Kaufman
4 Professional Drive
Suite 130
Gaithersburg, MD 20760

Motorola, Inc. 1
Semiconductor Group
Attn: R. Gurtler
5005 East McDowell Road
Phoenix, AZ 85008

Mount Edison USA, Inc. 1
Attn: Merritt Kastens
East Lake Road
Hamilton, NY 13346

NASA Headquarters 1
Solar Terr. System Division
Attn: Donald Calahan, Code Ret 1
600 Independence Ave., SW
Washington, DC 20546

NASA Headquarters 1
Attn: J. P. Mullin
Code RP-6, M/S B636
Washington, DC 20546

NASA Lewis Research Center 1
Attn: Dr. H. W. Brandhorst, Jr.
M/S 302-1
21000 Brookpark Road
Cleveland, OH 44135

National Bureau of Standards 1
Attn: David E. Sawyer
Bldg. 225, Room B-310
Washington, DC 20234

PRC Energy Analysis Company 1
Attn: Mr. Arie P. Ariotedjo
7600 Old Springhouse Road
McLean, VA 22101

Photon Power 1
Attn: C. Lampkin
10767 Gateway West
El Paso, TX 79935

RCA, Advanced Technology Labs. 1
Attn: M. S. Crouthamel
Building 10-8
Gamden, NJ 08102

Rockwell International 1
Energy System Group
Attn: Mr. B. L. McFarland
Dept. 714
8900 Desoto Ave.
Canoga Park, CA 91304

C. T. Sah Associates 1
Attn: Dr. C. T. Sah
403 Pond Ridge Lane
Urbana, IL 61801

J. C. Shumacher Company 1
Attn: Dr. Dennis Elwell
580 Airport Road
Oceanside, CA 92054

Sensor Technology, Inc 2
Attn: I. Rubin
21012 Lassen Street
Chatsworth, CA 91311

Silicon Technology Corporation 1
Attn: Dr. George S. Kachajian
P. O. Box 310
Oakland, NJ 07436

Siltec Corporation 1
Attn: T. Bonora
3717 Haven Avenue
Menlo Park, CA 94025

Siltec Corporation 1
Attn: Technical Library
3717 Haven Avenue
Menlo Park, CA 94025

Solarelectronics, Inc. 1
Attn: Jeffrey Mui
21 Rita Lane
P. O. Box 141
Bellingham, MA 02019

Solar Energy Research Institute 1
Attn: SEIC/LIBRARY
1617 Cole Blvd.
Golden, CO 80401

Solar Energy Research Institute 1
Photovoltaic Branch Bldg. 9/1
Attn: Ted Ciszek
1617 Cole Blvd.
Golden, CO 80401

Solar Energy Research Institute 1
Photovoltaic Program Office
Attn: D. Feucht
1617 Cole Blvd.
Golden, CO 80401

Solar Energy Research Institute 1
Photovoltaic Program Office
Attn: Dr. Tom Surek
1617 Cole Blvd.
Golden, CO 80401

Solar Energy Research Institute 1
Photovoltaic Program Office
Attn: Dr. C. Edwin Witt
1617 Cole Blvd.
Golden, CO 80401

Solar Power Corporation 1
Attn: P. Caruso
20 Cabot Road
Woburn, MA 01801

Solarex Corporation 1
Attn: Jerry Culik
1335 Piccard Drive
Rockville, MD 20850

Solarex Corporation 1
Attn: John V. Goldsmith
1335 Piccard Drive
Rockville, MD 20850

Solavolt International 1
Attn: William J. Kaszeta
P. O. Box 934
Phoenix, AZ 85062

Solec International, Inc. 1
Attn: Ishaq Shahryar
12533 Chadron Ave.
Hawthorne, CA 90250

Southern Methodist University 1
Institute of Technology
Electrical Engineering Dept.
Attn: T. L. Chu
Dallas, TX 75275

Spectrolab, Inc. 1
Attn: Dr. J. Minahan
12500 Gladstone Avenue
Sylmar, CA 91342

Spectrolab, Inc. 1
Attn: W. Taylor
12500 Gladstone Avenue
Sylmar, CA 91342

Spire Corporation 1
Patriots Park
Attn: Allen R. Kirkpatrick
P. O. Box D
Bedford, MA 01730

Spire Corporation 1
Patriots Park
Attn: R. Little
P. O. Box D
Bedford, MA 01730

Stanford Research Institute 1
Materials Research Center
Attn: Dr. Angel Sanjuro, G213
333 Ravenswood Avenue
Menlo Park, CA 94025

Stanford University 1
Center for Materials Research
Attn: Dr. Robert S. Piegelson
Stanford, CA 94305

State University of New York 1
College of Engineering
Department of Materials Science
Attn: Dr. Franklin F. Y. Wang
Stony Brook, NY 11794

Strategies Unlimited 1
Attn: John Day III
Suite 205
201 San Antonio Circle
Mountain View, CA 94040

Texas Instruments, Inc. 1
Attn: Dr. John Robinson
2906 Ricketts
Highway 75
Sherman, TX 75090

Tideland Signal Corp. 1
Attn: Mr. Carl Kotilla
P. O. Box 52430
Houston, TX 77052

Tracor MB Associates 1
Attn: Mr. A. L. Foote
Bollinger Canyon Road
San Ramon, CA 94583

TRW Systems Group 1
Attn: Paul Goldsmith
Bldg. M1/1334
One Space Park
Redondo Beach, CA 90278

Union Carbide Corporation 1
Linde Division
Attn: W. C. Breneman
P. O. Box 44
Tonawanda, NY 14150

Union Carbide Corporation 1
Electronics Division Tech Ctr
Attn: Dr. Hiroshi Morihara
3333 Index Street
Washougal, WA 98671

University of Delaware 1
College of Engineering
Attn: Professor Karl W. Boer
Du Pont Hall
Newark, DE 19711

University of Illinois 1
Materials Engineering
Chicago Circle Compus
Attn: Steven Danyluk
Chicago, IL 60680

University of Michigan 1
Attn: Raoul Kopelman
Dept. of Chemistry
Ann Arbor, MI 48104

University of Missouri-Rolla 1
Ceramic Engineering Department
Attn: Dr. P. Darrell Ownby
Rolla, MO 65401

University of Florida 1
Attn: Dr. F. A. Lindholm
219 Ginter Hall
Gainsville, FL 32611

University of Pennsylvania 1
Dept. of Electrical Eng. & Science
Attn: Professor Martin Wolf
308 Moore D2
Philadelphia, PA 19174

University of South Carolina 1
College of Engineering
Attn: R. B. Hilborn, Jr.
Columbia, SC 29208

University of South Carolina 1
College of Engineering
Attn: Dr. William Harrison
Columbia, SC 29208

U. S. Air Force 1
Aeropropulsion Lab.
Attn: Mr. Joseph Wise
AFAPL/POE-2
Wright-Patterson AFB, OH 45433

U. S. Coast Guard 1
R & D Center
Attn: Dr. F. Giovane
Avery Point
Groton, CT 06340

U. S. Department of Energy 1
Forrestal Building
Attn: R. Annan
1000 Independence Ave., SW
Washington, DC 20585

U. S. Department of Energy 1
Attn: Dr. Morton Prince M/S 5G026
Photovoltaic Energy Systems
1000 Independence Ave., SW
Washington, DC 20585

U. S. Department of Energy 1
Forrestal Building
Attn: Richard King
Photovoltaic Energy Systems
1000 Independence Ave., SW
Washington, DC 20585

U. S. Department of Energy 2
Technical Information Center + Repro
Attn: Doc. Control & Eval. Branch
P. O. Box 62
Oak Ridge, TN 37830

Varian Associates 1
Attn: Edward L. Jaye
611 Hansen Way
Palo Alto, CA 94306

Virginia Semiconductor, Inc. 1
Attn: Dr. Thomas G. Digges, Jr.
1501 Powhatan St.
Fredericksburg, VA 22401

AT&T Bell Telephone Laboratories 1
Attn: Joseph Mormbito
555 Union Blvd.
Allentown, PA 18930

Western Electric 1
Engineering Research Ctr.
Attn: Aline Akselrad
P. O. Box 900
Princeton, NY 08540

Southern California Edison 1
Attn: Nicholas Patapoff
P. O. Box 800
Rosemean, CA 91770

Pacific Gas and Electric 1
Attn: S. Hester
3400 Crow Canyon Road
San Ramm, CA 94583

Arizona State University 1
Attn: G. Schwuttke
TEmpe, AR

Georgia Institute of Technology 1
Attn: A. Rohatgi
School of Electrical Engineering
Atlantic, GA 30332